

THERMAL DIFFUSIVITY IN
FLUORIDE GLASSES

By

JOHN FREDERICK SNODGRASS

Bachelor of Science

Edinboro University of Pennsylvania

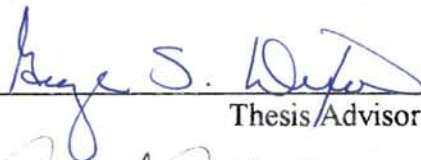
Edinboro, Pennsylvania

1991

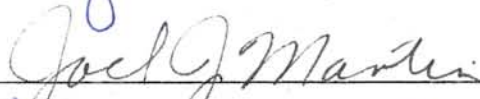
Submitted to the Faculty of the
Graduate College of the
Oklahoma State University
in partial fulfillment of
the requirements for
the Degree of
MASTER OF SCIENCE
May, 1996

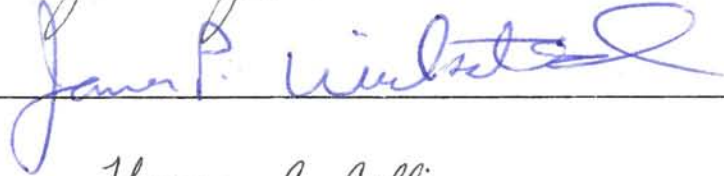
**THERMAL DIFFUSIVITY IN
FLUORIDE GLASSES**

Thesis Approved:



Thesis Advisor





Thomas C. Collins

Dean of the Graduate College

ACKNOWLEDGMENTS

I would like to express my appreciation to all the people responsible for helping me during my studies at Oklahoma State University. Foremost among these individuals is my thesis adviser, Dr. George S. Dixon. I would like to thank him for giving me the chance to learn and work in his laboratory as a graduate student, and for his advice, support and encouragement. I would also like to thank the other members of my committee, Dr. Joel Martin and Dr. James Wicksted.

My thanks and love go to my parents, family, friends, and my loving girlfriend Sandi Ulrich, all who have provided their constant love and support. Of my parents, David and Fay, and my brother Dave, I thank them for their interest, curiosity, and endless questions about my progress. I especially appreciated the question, "When are you going to get done writing your thesis?". Of Sandi, all I can say is without her vast knowledge of the English language this thesis might have been written in gibberish. I thank her for her support and never ending love. You people amused, abused and annoyed me, but certainly spared me from boredom.

Special thanks are extended to my good friends, Mike Furlough, Anne Georgalas, Cindy Porter, Jeff McCullough, Lynett Rock, George Kambouroglou, Patricia Watson and Karen Suhm, all who have suffered with me throughout my extended visit to Oklahoma. Without their support, the world of physics might have come crashing down around me.

TABLE OF CONTENTS

Chapter	Page
I. INTRODUCTION.....	1
• Amorphous Solids.....	2
• Structure of Glasses.....	7
• Continuous Random Network Model of Covalent Glasses.....	12
• Modified Random Network.....	16
• Einstein and Debye Models of Heat Transport.....	18
• Phonons in Glasses.....	20
• Raman Spectroscopy.....	26
• Statement of Purpose.....	31
II. EXPERIMENTAL PROCEDURE.....	32
• Samples.....	32
• Experimental Setup for Thermal Diffusivity.....	34
• Procedure for Thermal Diffusivity.....	35
• Experimental Setup for Raman Spectroscopy.....	42
• Procedure for Raman Spectroscopy.....	45
III. RESULTS and DISCUSSION.....	47
IV. CONCLUSION.....	62

REFERENCES..... 64

LIST OF TABLES

Table	Page
I. Sample Compositions.....	33
II. Physical Properties of the Glasses.....	53

LIST OF FIGURES

Figure	Page
1. The two general cooling paths by which a liquid can condense into the solid state. Route 1 is the path to the crystalline state. Route 2 is the path to the amorphous state.....	4
2. The schematic representation of the atomic arrangements in (a) a crystalline solid, (b) an amorphous solid, and (c) a gas.....	8
3. Comparison of X-ray derived RDFs of crystalline and amorphous germanium; c-crystal and a-amorphous solid.....	11
4. (a) The honeycomb lattice and (b) the decorated honeycomb. The topological structure of the honeycomb is the same as that of a layer in graphite or crystalline arsenic.....	13
5. Two-dimensional continuous random networks. A sketch of a three-fold-coordinated elemental glass is presented in a, while Zachariasen's (1932) diagram for an A_2B_3 glass is shown in b.....	15
6. The Modified Random Network (MRN) model for the structure of glass. The dashed bonds represent ionic interaction. The regions that are not shaded represent the modifier channels.....	17
7. The thermal conductivity as a function of temperature of crystalline quartz(I) and fused quartz(II).....	22
8. Average phonon mean free path as a function of temperature for various glasses and SiO_2 crystal.....	24
9. The diagrammatic representation of the Raman spectrum of carbon disulphide as an example of the Stokes lines verses the anti-Stokes lines.....	28
10. Illustrates a schematic representation of the high temperature experimental setup.....	36

11. Illustrates a schematic representation of the low temperature cryostat experimental setup.....	37
12. Typical temperature vs. time data. The upper curve is for the thermocouple closest to the heater and the lower curve is for the thermocouple farthest away from the heater.....	39
13. Plot of $\partial T/\partial t$ vs. $\partial^2 T/\partial x^2$ calculated from the data of figure 12. The slope of this curve is the thermal diffusivity, α	41
14. Schematic representation of the light scattering setup for the Raman spectrometer used in this experiment.....	43
15. Schematic representation of the sample chamber from figure 14. In this method the laser is directed at the sample from the side, top or bottom, and the sample is surrounded by mirrors to reflect as much light as possible into the slit of the spectrometer.....	44
16. Thermal diffusivity as a function of temperature for the ZBLAEu-147 sample. In addition, the individual contributions to the thermal diffusivity of the extended and localized phonons is shown.....	48
17. Thermal diffusivity as a function of temperature for the ZBLAH-144 sample. In addition, the individual contributions to the thermal diffusivity of the extended and localized phonons is shown.....	49
18. Thermal diffusivity as a function of temperature for the ZBLAE-331 sample. In addition, the individual contributions to the thermal diffusivity of the extended and localized phonons is shown.....	50
19. The thermal diffusivities as a function of temperature for all three samples.....	51
20. Raman spectrum of the ZBLAEu-147 sample. The main figure shows the full Raman spectrum for this sample. The arrows in the full spectrum point to the frequencies used in the multi-term Einstein approximation.....	54
21. Raman spectrum of the ZBLAH-144 sample. The main figure shows the full Raman spectrum for this sample. The arrows in the full spectrum point to the frequencies used in the multi-term Einstein approximation.....	55

22. Raman spectrum of the ZBLAE-331 sample. The main figure shows the full Raman spectrum for this sample. The arrows in the full spectrum point to the frequencies used in the multi-term Einstein approximation.....	56
23. Schematic representation of the thermally activated hopping of localized phonon process.....	58

CHAPTER I

INTRODUCTION

Thermal transport properties of glasses have presented an interesting set of research questions over the last twenty-five years. The thermal conductivity experiments of Zeller and Pohl[1] presented clear and unambiguous evidence that below the plateau region of approximately 1K the thermal properties of amorphous insulating solids differ remarkably from their crystalline counterparts.

The experiments of Zeller and Pohl[1] provide strong evidence that Debye-like phonons exist in glasses, and are scattered by additional excitations which can most simply be represented by the two-level-system (TLS) model, or more generally by highly anharmonic oscillators[3]. This model accounts for many of the properties of glasses at temperatures below the plateau region. In this picture the heat carriers are extended-state phonons, similar to the Debye Phonons of crystalline solids, and the TLS provide a scattering mechanism for them. On a more general level, an important consequence of the success of the TLS model has been the recognition that amorphous solids can support excitations that differ qualitatively, as well as quantitatively, from those ordinarily encountered in crystalline solids[2].

At temperatures above the plateau($\sim 5\text{K} < T < \sim 20\text{K}$), there is not yet a consensus on the nature of the phonons that provide the heat carriers nor on the elastic properties of the glass that may be needed for effective thermal transport by these models. The most successful current models suggest that some or all of the Raman-active phonons are

weakly localized by the disordered structure of the glass. The thermal transport process is one in which these localized phonons diffuse among neighboring localization sites by a random walk or hopping process[2].

In this thesis, a study of the thermal diffusivity between 80 and 500 K for a set of three fluoride glasses is presented. The two samples named ZBLAEu-147 and ZBLAH-144 consisted of a base compositional formula of $0.36(\text{BaF}_2) 0.57(\text{ZrF}_4) 0.01(\text{LaF}_3) 0.04(\text{AlF}_3) 0.02(\text{M})$ and doped with the modifier (M) of EuF_3 or HoF_3 , respectively. The third sample, ZBLAE-331, had the same composition as the other two with the exception of $0.025(\text{LaF}_3)$ and the modifier(M) being 0.05ErF_3 . The data obtained in this experiment will be analyzed and shown to adhere to the two-carrier model for thermal transport in glasses with localized phonons as the principal heat carriers in this temperature range introduced by Dixon and coworkers[2].

Amorphous Solids

Amorphous materials can be defined as those materials which are “topologically disordered” and which do not exhibit periodicity characteristic of crystals. Amorphous solids do not have the long-range orientational order characteristic of quasicrystals. For example, in a crystal state, all atomic positions are fixed when a few parameters are defined by position and distances. However, such a simple definition is impossible in both the gaseous and liquid states. To illustrate, fluctuations exist in the atomic distribution of liquids and gases in near-neighbor regions, but such fluctuations disappear at greater

distances. Naturally, the fluctuation in the atomic distribution in near-neighbor regions for liquids is larger than that of gases.

In the gaseous state, the atoms are distributed with a low average density and with mean free path which is long in comparison to the atomic size. In addition, the positional correlation of atoms is weak. However, the atoms do not mutually approach within the atomic core diameter a_0 due to the repulsion of the pair potential. In both the liquid and amorphous state, the atoms are randomly distributed in a nearly close-packed structure, and the mean free path of the atoms are short and proportional to the atomic size. This implies that the positional correlation of atoms is relatively strong within the near-neighbor region. Nevertheless, due to high atomic vibration, the average atomic configuration in the liquid state is more homogeneous than that of the amorphous state. In other words, the atomic configuration in the amorphous state has more rigid packing than that of the liquid state. Consequently, the term *amorphous state* (or solid) can be generally defined as any solid having a non-periodic atomic array.

Short of possessing the dynamic disorder characteristic of fluids, amorphous solids are among the most disordered of materials[7]. Amorphous and crystalline solids have two quite different solidification processes. As figure 1 shows, a liquid may either solidify discontinuously into a crystalline solid or continuously into an amorphous solid[6]. Figure 1 should be read from right to left since time runs in that direction during the course of the “quenching or temperature-lowering” experiment. A sharp break or bend in the Volume vs. Temperature curve, $V(T)$, marks a change of phase occurring with decreasing temperature. The first occurs when the gas condenses to the liquid phase at the boiling temperature T_b . Continued cooling now decreases the liquid volume in a

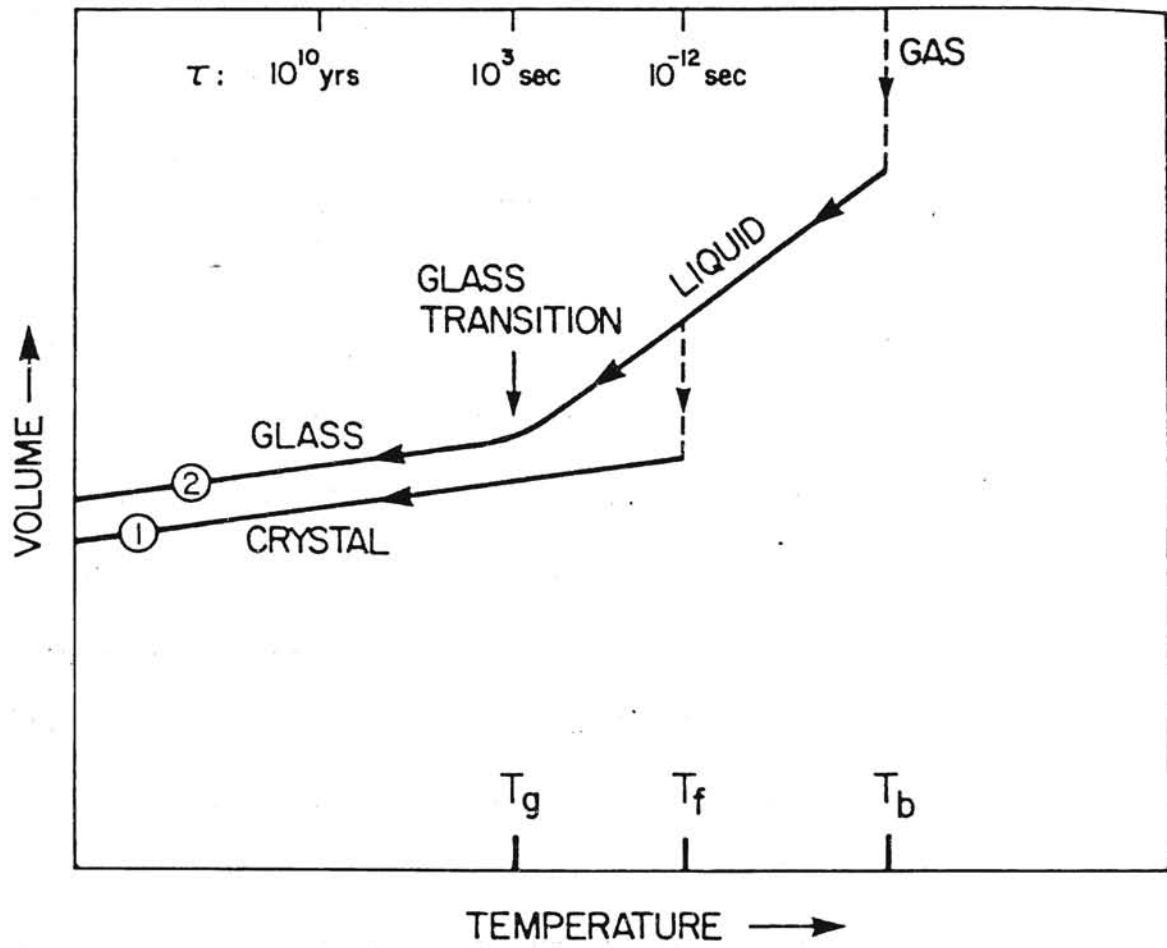


Figure 1. The two general cooling paths by which a liquid can condense into the solid state. Route 1 is the path to the crystalline state. Route 2 is the path to the amorphous state. (from ref. 6)

continuous fashion, the slope of the smooth $V(T)$ curve defining the liquid's volume coefficient of thermal expansion $\alpha = (1/V)(\partial V/\partial T)_P$. Eventually, when the temperature is low enough, a liquid to solid transition takes place. The solid then continues to $T = 0$, with a small slope which corresponds to the low value of the expansion coefficient, α , which characterizes a solid.

Almost all materials can be prepared as amorphous solids. One key to which path a liquid will follow in solidifying is the speed or "how fast the melt is cooled or quenched"[6]. Crystalline solids are usually fabricated by the use of very low cooling rates. Low cooling rates are necessary since crystallization requires time for crystalline centers to first form and then grow at the expense of the liquid which may have different local order. Furthermore, the liquid to crystal transition is marked by a discontinuity at T_f (freezing point) in the $V(T)$ curve, which is due to the abrupt contraction of the volume of the crystalline solid. In a quenching experiment carried out at a sufficiently low cooling rate, this is usually the route taken to arrive at the solid state. Conversely, if the cooling rate of the melt is high enough or fast enough, T_f is bypassed, and the liquid phase endures until a lower temperature T_g , called the glass transition temperature, is reached. In this case, the second solidification scenario is realized in which an amorphous solid or glass is formed.

The term *glass* has conventionally been reserved for an amorphous solid actually prepared by "quenching or temperature-lowering" the liquid melt in the experiment[6]. Unlike the crystalline solid, there is no $V(T)$ discontinuity in the amorphous solid, but there is a trend in both scenarios to assume small slopes that are characteristic of low thermal expansion[6]. In this temperature range, the viscosity of the melt increases rapidly,

approaching that of a crystalline solid. During the time the liquid is cooled from T_f to T_g , it is prone to nucleation and growth of crystallites. Therefore, in the preparation of amorphous solids, the cooling must proceed “far enough”, in the sense that the quench must be taken to below the glass transition temperature ($T < T_g$), and “fast enough” in the sense that $T_g < T < T_f$ must be crossed in a time too short for crystallization to occur[6].

Thus, the essential ingredient in the preparation of an amorphous solid is *speed*. As soon as the temperature of the liquid is lowered to T_f , it may take the path to the solid state and crystallize. To accomplish this, one can block the kinetic paths that lead to crystallization. This can be done in two ways: by rapidly cooling the melt to block thermal motion of mixture or by placing the system in a state where local rearrangement to crystallization requires a large energy or entropy change. This entropy change only occurs in the intermediate states between local order and the local arrangement consistent with translational symmetry. If the melt’s temperature can be taken below T_g before crystallization has had time to occur, the undercooled liquid solidifies as a glass and remains in this form essentially indefinitely[6].

Glass formation, therefore, is a matter of *bypassing crystallization*. The channel to the crystalline state is evaded by quickly crossing the dangerous regime of temperature between T_f and T_g and achieving the safety of the amorphous solid state below T_g . Throughout the temperature interval $T_g < T < T_f$, the liquid is “at risk” with respect to nucleation and growth of crystallites.

As previously mentioned, for a material to be prepared as an amorphous solid, cooling must proceed “fast enough and far enough.” When these conditions exist, the liquid to glass transformation occurs homogeneously throughout the material.

In contrast, during crystallization, heterogeneous pockets of the solid phase appear abruptly within the liquid and then grow at its expense. Without the intervention of crystallization[6], all liquids would form glasses if sufficiently undercooled.

Structure of Glasses

For an amorphous solid, the essential structural difference with respect to that of a crystalline solid is the absence of *long-range order* (periodicity). This difference complicates the study of glasses more than their crystalline counterparts where an underlying periodic lattice exists from which one can describe the whole crystalline solid on the basis of a few atoms. Figure 2 presents schematically the characteristics of the atomic arrangements in glasses as opposed to crystals. Also included, as an additional reference point, is an illustration of the arrangement in a gas. Notice that two-dimensional crystals, glasses, and gases are represented, but the essential points to be noted carry over to their actual, three-dimensional, physical counterparts.

The lack of long-range order in glasses implies randomness at large separations. Knowing the positions of a few atoms does not help to locate, as it does in a crystal, the positions of distant atoms. However, this does not mean that glasses are structurally completely random at all length scales. As seen in figure 2*a* and 2*b* the atomic positions in the glass are not randomly distributed in space. Randomness is a trait more properly associated with figure 2*c*. Each atom can be found at any location, independent of the positions of all other atoms. But in figure 2*b*, a high degree of *local* correlation is seen.

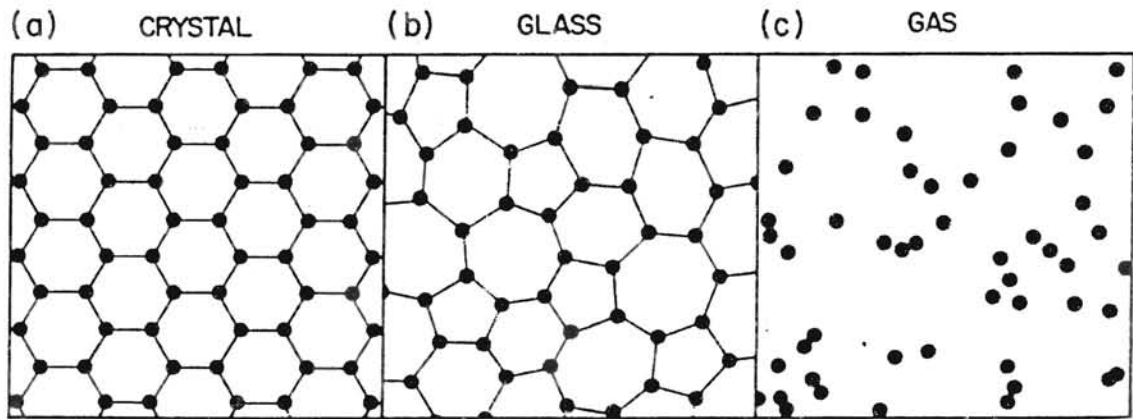


FIGURE 2. The schematic representation of the atomic arrangements in (a) a crystalline solid, (b) an amorphous solid, and (c) a gas.

In other words, glass exhibits a high degree of *short-range* order. Each atom has three nearest neighbors at nearly the same distance from it. The nearest-neighbor atoms are connected by lines in figure 2a and 2b. The “bond angles” formed where these lines meet at an atomic position and are correspondingly *nearly* equal.

In the crystalline case of figure 2a, the nearest-neighbor separations and bond lengths are *exactly* equal, rather than *nearly* equal as in the glass. The *exactly* equal bond lengths can be considered to be a “formula cell” introduced by Dixon and coworkers[2] as the smallest number of atoms in which each element is represented in the same proportion as in the sample as a whole. The “formula cell” structure can not be seen throughout figure 2b at long-range but can be seen at shorter-ranges. Thus glasses share a high degree of *short-range order* with crystals. As in crystals, this is a consequence of the chemical bonding responsible for holding the solid together[6,7]. The importance of short-range order in glasses can be seen in those applications where a crystalline solid can be replaced by its glass counterpart. This is due to the fact that glassy materials often share the same coordination numbers and nearest-neighbor separation as their crystalline counterparts[7].

The atomic structure of glasses can be describe in terms of increasing length scales. Two such length scales can be distinguished by short-range order(SRO) and medium-range order(MRO) from the structure of a glass. Short-range order encompasses a length scale from 2 to 3 Å and is associated with the nearest-neighbor environment of atoms. For the case of covalently-bonded glasses, the simplest description of SRO is in terms of local coordination polyhedra and their interconnectivity[7]. Thus, SRO can be characterized in terms of intra-polyhedral factors, such as the 2-body correlation quantities: r , the nearest-

neighbor bond length, and z , the coordination number. The coordination number z of a particular atom is the number of the nearest neighbor atoms which surround that atom in the solid. The coordination number z is the most valuable piece of structural information which provides evidence for a dominant role of covalent bonding ($z \leq 4$) in the coupling of nearest-neighbor atoms[6]. By generalizing the idea of a single coordination number to a sequence of numbers embracing “shells” of neighbors at distances beyond the nearest ones, one is led to a more substantial structural characterization called the radial distribution function (RDF)[6]. In figure 3, direct evidence of the existence of SRO in glasses, in the form of well-defined nearest neighbor and next-nearest neighbor coordination shells, is provided by the first and second peaks in the X-ray-derived RDF of amorphous germanium. Notice that figure 3 shows a superposition of this RDF for germanium crystalline powder(c-Ge) and the RDF for the germanium amorphous solid(a-Ge). This crystal/glass comparison is especially useful because both curves were obtained under the same experimental conditions and by means of the same analytical transformation procedure[6]. However, the absence of long-range order manifests itself in the fact that, for glasses, discernible peaks in the RDF rarely occur beyond third-nearest neighbors.

While the SRO of glasses is well known, the same cannot be said about medium-range order(MRO). Presently, the terms used to describe MRO are not well defined which causes great controversy about what comprises the MRO of glasses[27]. This is due to the fact that while diffraction experiments reveals a wealth of information about SRO, they result in almost no information about MRO because of the absence of long-range order. As an example of the level of disagreement that exists in characterizing

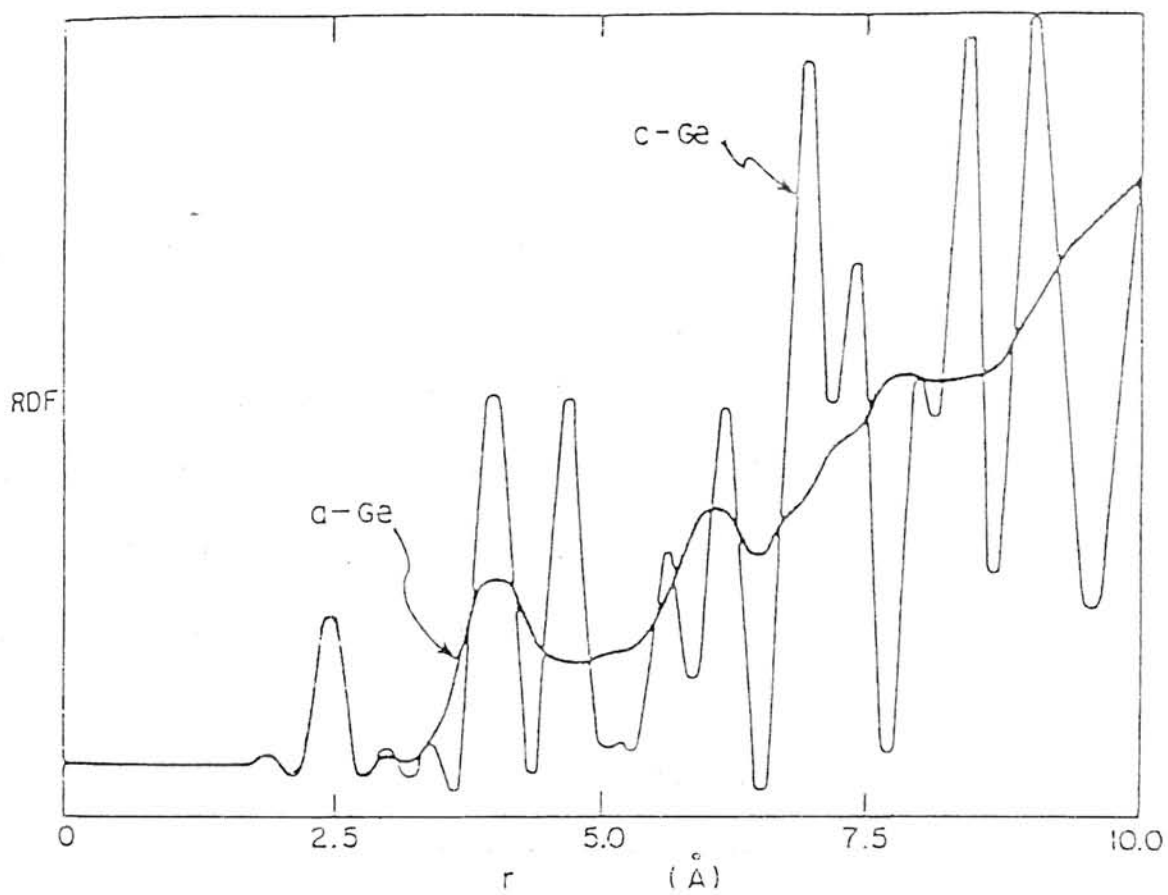


FIGURE 3. Comparison of X-ray derived RDF's of crystalline (c-crystal) and amorphous germanium (a-amorphous solid).

MRO, reference 27 considers the length scale of 3Å to 5Å as part of SRO for most materials, while in reference 7 this range is included as part of the local-scale MRO.

The main concept of this section was to become more familiar with the many descriptions of glasses. While much more can be said about the classification and description of different length scales as a definition of glasses, the subject area is too large for the scale of this paper and will not be discussed further.

Continuous Random Network Model of Covalent Glasses

In 1932 W.H. Zachariasen, in his classic paper entitled “The Atomic Arrangement in Glass,” set forth what has since become known as the continuous-random-network model (henceforth, CRN) for the structure of covalently bonded amorphous solids[6]. The essential characteristics of CRN structures are revealed by comparing figure 4 and figure 5.

Figure 4 represents two different cartoons representing covalent structures of crystalline solids. The honeycomb lattice of figure 4a is the two-dimensional covalent graph corresponding to a layer of bonded carbon atoms in graphite. Figure 4b represents the “decorated” honeycomb lattice, as it is derivable from a honeycomb lattice by replacing each bond by a pair of bonds to an intervening twofold-coordinated “bridging” atom[6].

While the two covalent cartoons of figure 4 represent periodic structures, figure 5 shows a corresponding pair of cartoons which represent continuous random networks;

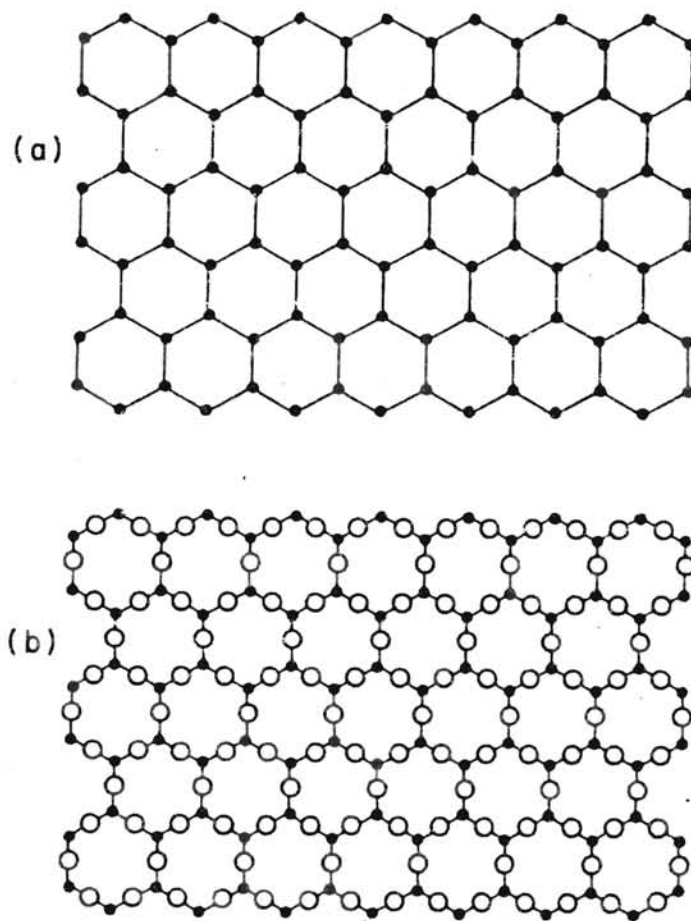


FIGURE 4. The honeycomb lattice (*a*) and the decorated honeycomb (*b*). The topological structure of the honeycomb is the as that of a layer in graphite or crystalline arsenic.

each of these noncrystalline structures has the same short-range order as its crystalline counterpart in figure 4. To begin with the simpler case, the elemental network glass of figure 5a shares the following features in common with the honeycomb crystal lattice:

1. $z = 3$, each atom is threefold coordinated.
2. Nearest-neighbor distances (i.e., bond lengths) are constant, or nearly so.
3. Both structures are “ideal” in admitting no dangling bonds.

Both networks are indefinitely extendible and no notice is taken here of surface effects.

Actually statement 3 is implied by statement 1, but it is worth separate mention because of its chemical significance[6]. Statement 2, as emphasized by Zachariasen, is the condition which ensures that the energy of the covalent glass is little different from that of the crystal. The two fundamental ways in which the crystalline and the continuous-random networks distinctly differ from each other are:

4. A significant spread in bond angles, not permitted in the crystal, is characteristic of the CRN structure.
5. Long-range order is absent for the CRN glass.

There is an additional degree of latitude in the presence of a second type of bond angle that occurs at the bridging atom. Since the bond angle at a twofold-coordinated atom is expected to be much softer (i.e., much less costly in energy to deform) than that at a threefold-coordinated atom, all of the bond-angle leeway may be supposed to be taken up at the bridging atoms[6]. Thus statement 4 now applies only to the soft bond angles in the network, while the stiff bond angles may be lumped together with the bond lengths in statement 2 as little different in the CRN glass from their values in the crystal. This is the case in figure 5b. Also evident in a comparison of this structure with that of figure 5a is

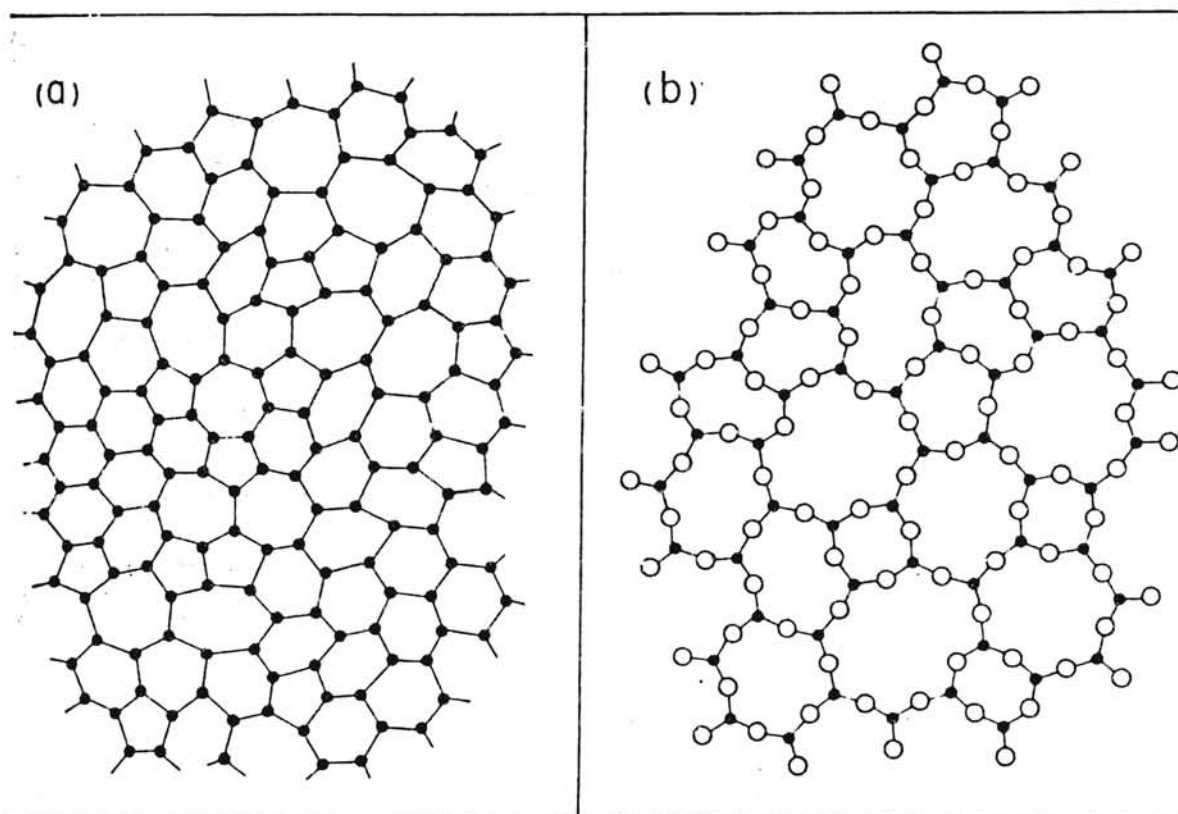


FIGURE 5. Two-dimensional continuous random networks. A sketch of a three-fold-coordinated elemental glass is presented in (a), while Zachariasen's (1932) diagram for an A_2B_3 glass is shown in (b).

the relative ease, because of the bends permitted at the bridging atoms, of developing a covalent network without bond-length distortion in the case of the compound[6].

Modified Random Network

Though glasses present complexities not found in crystals, they possess specific properties which make them advantageous to crystals. For one, the compositional flexibility of glasses allows for the study of different types of additives over a continuous range of concentrations without running into solubility limits. Furthermore, the structural changes created in the glasses by the additives enable one to study transport-structure correlations more readily than in crystalline solids[7]. This has sparked the development of the model, based on the same principles as Zachariasen's CRN model, called the Modified Random Network Model (MRN).

In the MRN model, glass-modifying oxides are believed to micro-segregate from glass-forming oxides at the atomic level as shown in figure 6. The effect of modifiers are to simultaneously change the network structure and bonding which affects its rigidity, net charge, and distribution of interconnected interstices. These changes are reflected in the physical properties of the glass[7]. Network modifiers induce charges in the network by introducing ionic bonds between the positively-charged interstitial modifier cations and the now negatively-charged covalent chains.

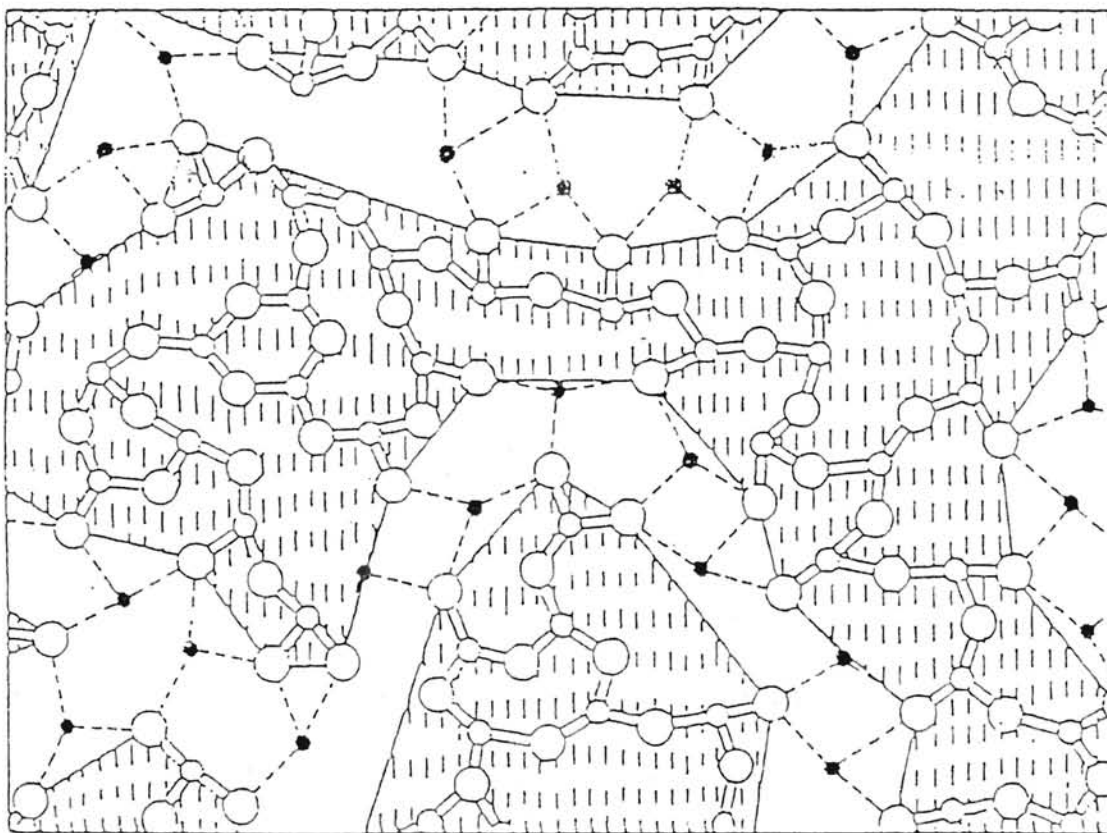


FIGURE 6. The Modified Random Network (MRN) model for the structure of glass. The dashed bonds represent ionic interaction. The regions that are not shaded represent the modifier channels.

Einstein and Debye Models of Heat Transport

In the classical Einstein model of lattice vibrations, based on the work of Petit & Dulong[18], every atom contains the vibrational energy $3k_B T$, where k_B is Boltzmann's constant and T the absolute temperature. This leads to a temperature-independent specific heat $3k_B n$, where n is the number density of atoms (number per volume). The limits of this picture were demonstrated by H. F. Weber[19] in 1875, who showed that the specific heat approached this so-called Dulong-Petit value only at high temperature. By extending the measuring temperatures below room temperature, he observed a decrease in specific heat of diamond by as much as a factor of ten[19].

With the experimental data of Weber, Einstein[20] took 32 years to recognize that the atomic vibrations were quantized. These "Einstein Oscillators", as they are now known, have a specific heat that approaches the Dulong-Petit value at high temperatures and that decreases exponentially at low temperatures. Therefore, in Einstein's model the thermal conductivity should decrease with decreasing temperature. However, a dilemma occurred when another experiment was conducted by A. Eucken, in which he observed the thermal conductivity to increase with increasing temperature at low temperatures[17].

The way out of the fundamental dilemma inherent in the Einstein model was suggested by Debye[21] and by Born & von Karman[22]. These authors argued that atoms in a solid do not oscillate as isolated entities, but collectively as propagating waves. Debye treated these elastic waves as dispersionless in a way identical to the electromagnetic waves in an empty cavity; the only differences were that he included longitudinal waves, and that he limited the number of normal modes to $3n$, where n is the

density of atoms in a three-dimensional solid[17]. With these assumptions, he was able to predict the specific heat of solids and found agreement with the measurements, whereas Einstein's theory employed the Einstein frequency as a free parameter. Debye was also able to explain why at low temperatures the specific heat decreased less rapidly than predicted by Einstein's lattice vibration model (Debye's T^3 dependence of the specific heat)[17].

A very important success of the elastic wave theory was that it opened the way to a qualitative understanding of the observed high thermal conductivity of dielectric crystals, and also of its temperature dependence. In analogy to the kinetic theory of gases, Debye[23] wrote the thermal conductivity Λ as

$$\Lambda = 1/3 C_V V L \quad (1-1)$$

where C_V is the specific heat (per volume), V the wave velocity, and L the mean free path between collisions with lattice defects and other waves. A mean free path of the order of 100 Å or a few tens of wavelengths, was required to explain Eucken's findings for crystalline solids. A rapidly decreasing scattering probability could be expected to more than compensate for the decreasing specific heat at decreasing temperatures, thus leading to an increase of the thermal conductivity[17]. Some of the important scattering mechanisms for elastic waves and their study through measurements of heat transport are reviewed below.

Phonons in Glasses

The thermal conductivity experiments of Zeller and Pohl[2] initiated a train of investigations that culminated in the two-level-system (TLS) model which accounts for many properties of glasses at temperatures below the plateau region($\sim 5\text{K} < T < \sim 20\text{K}$). In this picture, the heat carriers are extended-state phonons, similar to the Debye phonons of crystalline solids, and the TLS provide a scattering mechanism for the phonons[10]. Zeller and Pohl[1] were the first to present experimental evidence that the thermal properties of amorphous solids differ remarkably from their crystalline counterparts at low temperature.

Thermal transport properties of glasses have presented an interesting set of research questions, starting from Zeller and Pohl's experiments, over the last few decades. The research investigation concentrated on the behavior of the thermal conductivity and specific heat as a function of temperature, and the understanding and description of the processes which may or may not contribute to their behavior. While it has been well established[3,10,12,13,14] that phonons are responsible for the thermal diffusion in glasses, there is much disagreement as to how these phonons interact with each other and with other intrinsic properties of the material to give the observed behavior in the thermal conductivity[3]. While numerous models have been put forth since then, only those models which are generally accepted as representing the behavior of thermal conductivity in their respective temperature range will be briefly mentioned.

To begin, figure 7 displays the thermal conductivity as function of temperature of crystalline quartz(I) and fused quartz(II). The behavior of these two materials is vastly

different although they have the same chemical composition. In particular, the thermal conductivity of the amorphous solid is several orders of magnitude smaller than its crystalline counterpart[1]. Furthermore, it has been found that for a large variety of amorphous solids the thermal conductivities are very similar to the form shown in figure 7 and differ in magnitude within a factor of ten or less[3,11]. In contrast, the thermal conductivity in crystalline solids can vary by as much as five orders of magnitude, with correspondingly different temperature dependencies[11]. The thermal conductivity curve for amorphous materials can be divided into three distinct regions, A, B, and C, which are seen in figure 7. The scope of our experiments extends well into region A. Regions B and C will also be briefly discussed where the processes believed to be responsible for the behavior of the thermal conductivity occur.

For temperatures corresponding to region C of approximately less than 5 K, Zeller and Pohl[1] showed that the thermal conductivity varied as T^2 which was interpreted as due to a mean free path for phonons going as ω^{-1} . This T^2 behavior was first explained successfully through a model put forth by Anderson and coworkers[12] where low frequency extended phonons, similar to Debye phonons of crystalline solids, are scattered off localized two-level systems[3,13]. The temperature region below 1 K has attracted a great deal of attention. In this region the thermal conductivity varies as T^n , with n ranging between 1.8 and 2.0 depending on the chemical composition of the glass. The scattering is believed to be due to low energy excitations that have been observed through a specific heat anomaly that varied almost linearly with temperature[17]. It has been suggested that these excitations are caused by tunneling of atoms or groups of atoms between nearly identical sites in the amorphous lattice with an almost uniform density of states[25,26].

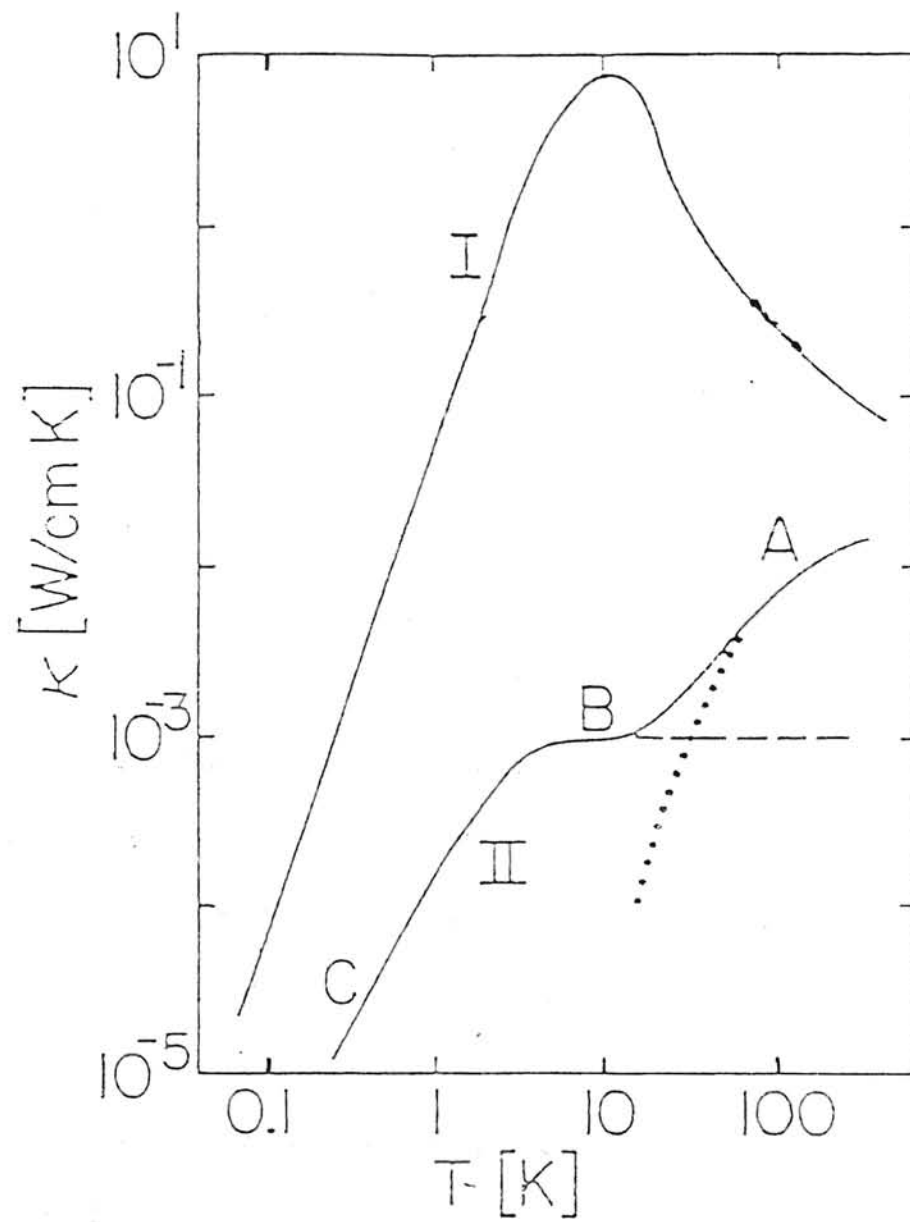


FIGURE 7. The thermal conductivity as a function of temperature of crystalline quartz(I) and fused quartz(II).

The details of the thermal conductivity are produced by phonons resonantly scattering off these states.

In region B, the plateau, where $\sim 5\text{K} < T < \sim 20\text{K}$, depending on the material, the thermal conductivity is independent of temperature. This plateau region is believed to include a mobility edge[13] or crossover frequency, ω_c , [12,14] where phonons with $\omega < \omega_c$ are extended states and those with $\omega > \omega_c$ are localized. The excited extended phonons are in the Dulong-Petit region, and so their contribution to the thermal conductivity is constant. This results in the plateau when coupled with a constant sound velocity and mean free path for the phonons with frequencies less than ω_c [13,14]. Figure 8 shows that the mean free path of the phonons (assuming all are extended states) decreases dramatically in the vicinity of the plateau region to within a few atomic spacings. The fact that the phonon mean free path becomes so strongly frequency dependent from a dependence of ω^{-1} at the lowest temperature region to an ω^{-4} dependence in the vicinity of the plateau, is still unclear. Jagannathan and coworkers[14] have attributed this phenomenon to Rayleigh-like scattering and anharmonic coupling between the extended state phonons and localized states. Some other literature suggests and supports the localization of certain phonons, mentioning that the mobility edge or crossover frequency is seen to occur approximately where the Ioffe-Regel condition is satisfied, which is generally accepted as signaling vibrational localization[10,14].

In region A, as the temperature increases above the plateau, the thermal conductivity increases approximately linearly. This behavior is attributed to phonon assisted hopping of the localized vibrational modes[10,13] or phonon-induced fracton-hopping[12,14]. In particular, as the temperature for frequencies $\omega > \omega_c$ increases, a

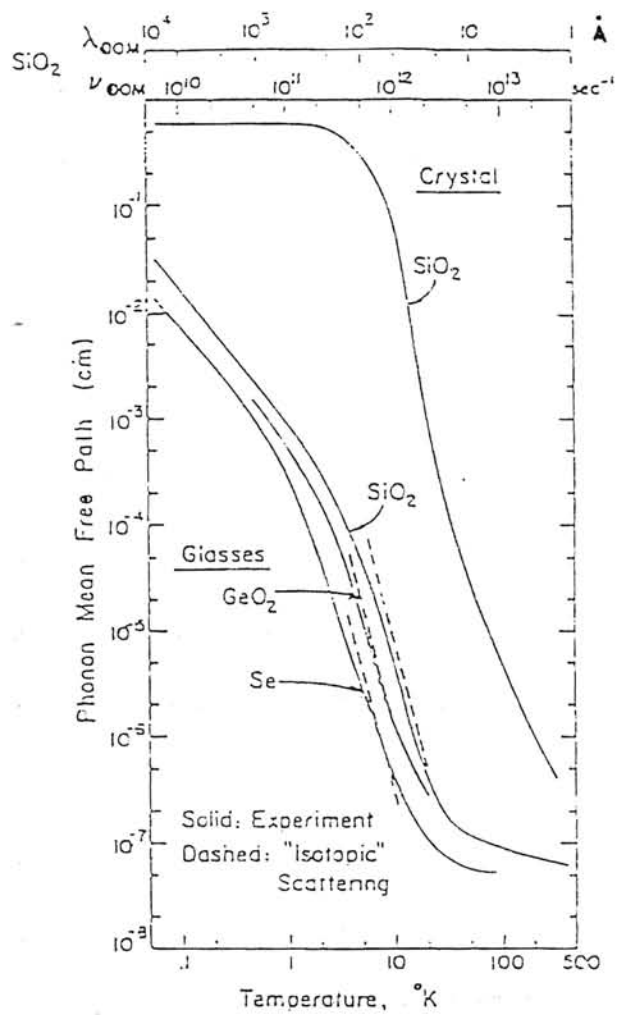


FIGURE 8. Average phonon mean free path as a function of temperature for various glasses and SiO₂ crystal.

significant number of localized modes are thermally excited and their hopping contributes to an increase in the thermal conductivity above the plateau value[14].

The anharmonic mechanism can have two results, absorption or emission of a photon. If absorbed either two phonons are created or one phonon is created and a second phonon of lower energy is destroyed. The emission of a photon either destroys two phonons or destroys one phonon and creates a second phonon of lower energy[15]. In 1929, Peierls[24] showed for the three phonon anharmonic process that two conservation laws had to be obeyed, one of the laws is:

$$\hbar\omega_1 + \hbar\omega_2 = \hbar\omega_3 \quad (1-2)$$

where ω_i is the (angular) frequency of the quanta and \hbar is Plank's constant divided by 2π ; this equation expresses the conservation of energy.

Alexander and coworkers[16] derived an expression for the contribution of this three phonon anharmonic process to the thermal conductivity. In their derivation, they assumed glasses are fractal in nature. They also introduced a fracton-hopping formulation as an additional heat-carrying channel above the plateau region. This introduction generated a linear increase in thermal conductivity with increasing temperature throughout their experiment. Though they assumed a fractal nature of glasses, Graebner and coworkers[10] point out that, in addition to the lack of evidence of the fractal nature of bulk glass, the assumption is not needed to explain the phonon assisted hopping of the localized modes above the plateau.

To summarize, crystal elastic waves, or phonons in the quantum picture, can lead to a very satisfactory description of the observed phenomena. In contrast, this same picture is incorrect in amorphous solids except at low temperatures or for long

wavelengths[17]. Lattice vibrations, as they are thermally excited above $\sim 30\text{K}$, appear to be more appropriately described as localized Einstein oscillators: the heat is being carried through the lattice by a random walk, rather than by wave-like motion. It is not understood, however, why these oscillators are so heavily damped in all glasses.

At temperatures below 30K , thermally excited elastic waves occur also in glasses. In fact, their scattering mean free path always exceeds 100 wavelengths when less than a few Kelvin, corresponding to phonon frequencies less than one terahertz[17]. However, in this energy range, some additional excitations have been found in all glasses. These excitations are localized and are most likely tunneling states (TLS). Their physical origin is also not completely understood. In conclusion many aspects of the vibrational spectrum of glasses over the entire frequency range are still poorly understood and require further study.

Raman Spectroscopy

The Raman process was first predicted from theoretical considerations by Smekal in 1923 and was discovered by C. V. Raman five years later[8]. The effect is described as an inelastic, non-resonant light scattering process in which an incident photon, or light quantum, interacts with matter. The result is the emission of a photon of different frequency than the incident photon and either the creation or annihilation of a phonon, or quantum of lattice vibration.

When a sample is irradiated with monochromatic radiation, a small portion of the incident radiation is scattered from the main direction of propagation. The largest percentage of this represents Tyndall scattering caused by dust particles or imperfections in the sample[8]. These types of scattering are considered elastic, since the radiation is scattered at the same frequency as that of the source.

If the light illuminating the sample is monochromatic and the scattered light is examined with a spectrometer, a series of emission lines will be seen. The strongest line appears at the frequency of the exciting monochromatic light and is due to Rayleigh elastic scattering. Symmetrically placed on either side of the Rayleigh line are a number of very much weaker lines, these being the Raman emissions. The Raman emissions on the low frequency side of the Rayleigh line are called the Stokes lines, and are of higher intensity than the anti-Stokes lines, which lie on the high frequency side[9]. Figure 9 shows the diagrammatic representation of the Raman spectrum of carbon disulphide as an example of the Stokes lines versus the anti-Stokes lines.

This intensity difference between the two sets of Raman lines arises because of the population difference between the different vibrational energy levels of the molecule. At room temperature there will be many more molecules in the ground vibrational state than in the higher vibrational states. Therefore the incoming light is more likely to interact with a molecule in the ground state and excite it to a higher vibrational state than it is to collide with a molecule in one of the higher energy states, causing it to lose energy and fall back to the ground state. If the light excites the molecule to a higher vibrational state it will lose energy and appear with a lower frequency; conversely, if it brings about a downward transition it will gain energy and appear at a higher frequency[9].

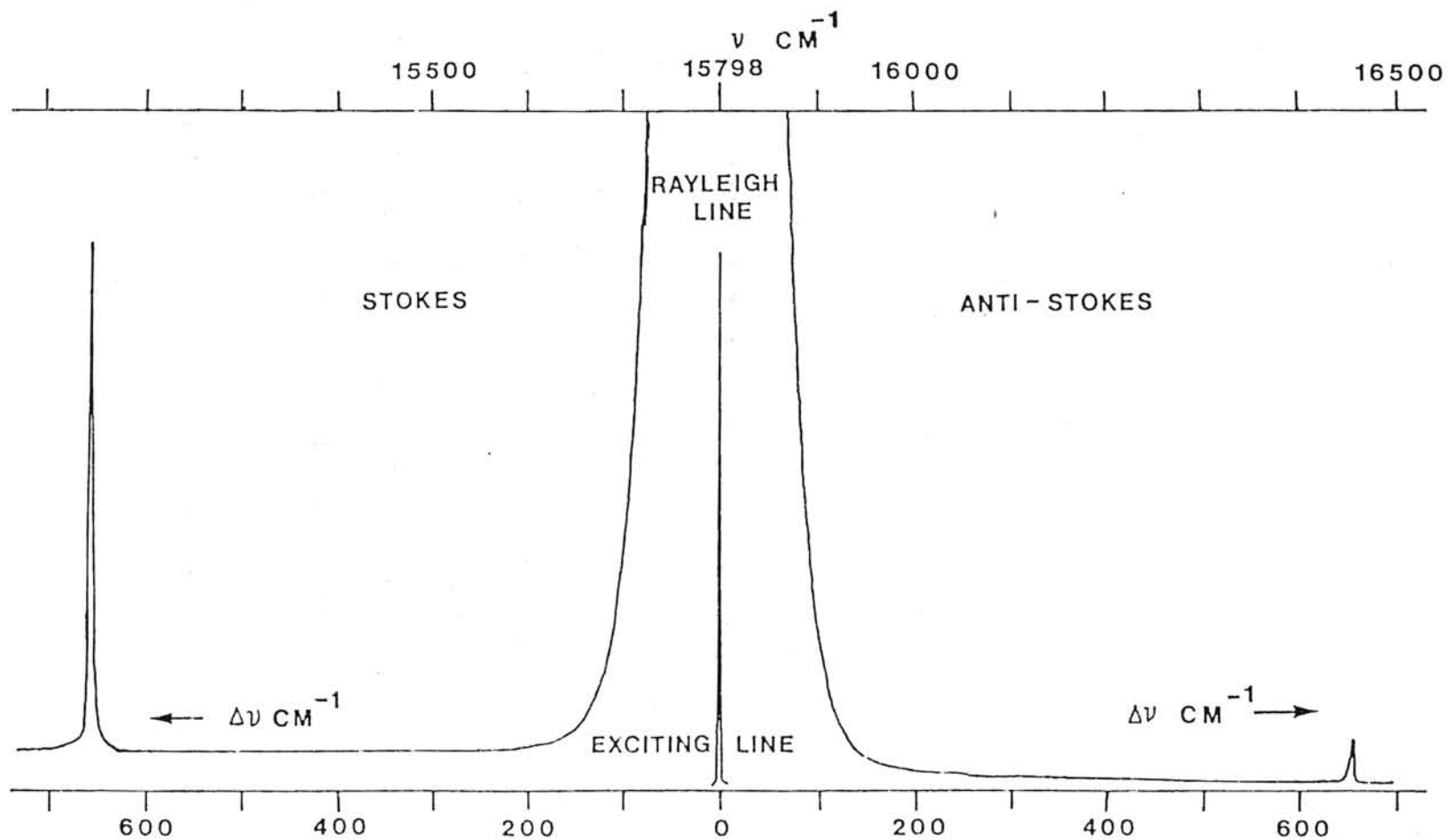


Figure 9. The diagrammatic representation of the Raman spectrum of carbon disulphide as an example of the Stokes lines versus the Anti-Stokes lines. (from ref 9)

The displacements of these lines from the Rayleigh line ($\Delta\nu$), measured in wavenumbers (cm^{-1}) are found to correspond to the frequencies of the molecular vibrations. These frequencies can sometimes be measured by absorption spectroscopy in the infrared. The infrared and Raman spectra obey different selection rules, so both are necessary if the maximum amount of information is to be obtained about a molecule.

The activity of a particular vibrational mode in the infrared region is dependent upon whether or not there is a change in the dipole moment during the vibration. For a mode to be Raman active there must be a change in the polarizability of the molecule during the vibration. This change can be considered as being a change in the shape of the electron cloud surrounding it[9].

Inelastic Raman scattering is considerably weaker than Tyndall or Rayleigh scattering. It is caused by changes in the polarizability of the sample. Raman scattering is considered inelastic because the scattered radiation is of a different frequency than that of the source. The intensity of the scattered light is extremely weak, approximately 10^{-8} times the intensity of the source[8]. The Raman scattering is directly proportional to the intensity of the incident light source; the higher the power that can be concentrated into a particular volume of sample, the more intense will be the recorded spectrum. Therefore very high power lasers are used to bring weak spectra up to a level where they can be recorded photo-electrically.

The Raman scattering is proportional to the fourth power of the frequency of the laser line exciting the spectrum -- this means that a red laser will be less efficient as a source for Raman spectroscopy than a green one[9]. As the frequency in wavenumbers is obtained by dividing the frequency in hertz by the velocity of light, the scattering is also

proportional to the frequency in wavenumbers. For example, changing from excitation of the spectrum by a 100 mW krypton ion laser operating at 14783 cm^{-1} (6471 \AA) to a 100 mW argon ion laser operating at 20487 cm^{-1} (4880 \AA) causes an increase of scattering efficiency of $(20487 / 14783)^4 \approx 3.7$ times[9].

It is important to note that most absorption or emission spectroscopy involves scattering in which the radiation is in resonance with the energy level transition of the material. Raman spectroscopy, however, is due to the scattering of non-resonant absorption or emission, and it is the frequency shift that gives information about the energy level transitions. In Raman scattering, the scattered photon brings extra information away with it, including information on rotational and vibrational transitions of the material[8].

In the Raman effect, a photon with initial energy $h\nu_0$ interacts with a molecule, resulting in the scattering of a photon of energy $h\nu_s \neq h\nu_0$ and the creation or annihilation of a phonon. The Raman effect must follow the law of conservation of energy, so that in a Stokes transition, where $h\nu_s < h\nu_0$, a phonon of energy $h\nu_0 - h\nu_s = h\nu$ is created. Likewise, in an anti-Stokes transition, where $h\nu_s - h\nu_0 = h\nu$ is annihilated. Thus, the Raman effect follows the selection rule

$$\nu_0 = \nu_s \pm \nu \quad (1-3)$$

where ν_0 , ν_s , and ν refer to the frequencies of the incident photon, scattered photon, and phonon, respectively. If there is no such phonon with energy $h\nu$, then the corresponding transition from $h\nu_0$ to $h\nu_s$ is forbidden.

Statement of Purpose

The purpose of this experiment was to track the effect of various rare earth elements being doped on the baseline composition set of fluoride glasses as it is inserted into the network. Specifically, as the three different rare earth materials were added to the baseline the thermal diffusivity as a function of temperature was examined in the temperature range of 80-500K. The data was analyzed using a two-carrier model for thermal transport by extended phonons, and thermally activated hopping of localized phonons. Within the two-carrier model, a Debye approximation is used to calculate the heat capacity of the extended modes, while a multi-term Einstein approximation using vibrational modes obtained from Raman data is used to calculate the total heat capacity of the three samples.

CHAPTER II

EXPERIMENTAL PROCEDURE

The Samples

Heavy metal fluoride glasses have proved to be excellent hosts for both rare earth and 3d transition metal ions. In addition, their potential as light guides is at present unexcelled. These glasses are especially promising for optical display devices, laser hosts, and electroluminescence panels. Numerous defects and impurities can be incorporated in the glasses which can absorb or emit light. In this thesis, the fluoride glasses were doped with three rare earth materials consisting of europium(Eu), holmium(Ho), and erbium(Er)

The three fluoride glass samples studied were doped with different concentrations of the rare earth elements. The samples used were ZBLAEu-147, ZBLAH-144, and ZBLAE-331 prepared at Hanscom Air Force Base, Massachusetts. The two samples named ZBLAEu-147 and ZBLAH-144 consisted of a base compositional formula of $0.36(\text{BaF}_2) 0.57(\text{ZrF}_4)0.01(\text{LaF}_3)0.04(\text{AlF}_3)0.02(\text{M})$ and doped with the modifier (M) of EuF_3 or HoF_3 , respectively. The third sample, ZBLAE-331, had the same composition as the other two with the exception of $0.025(\text{LaF}_3)$ and the modifier(M) being 0.05ErF_3 . The samples and their properties are listed in table 1 for easy reference.

Each sample was cut into rectangular parallelepipeds, typically $3 \times 3 \times 10 \text{ mm}^3$ in dimension. The first step in the experiment was to take the data for the thermal properties of each sample. The procedure for this is described below in the next section. Once all

TABLE I. Compositions of Samples.

Glass Sample	BaF₂	ZrF₄	LaF₃	AlF₃	Active Ion
ZBLAEu-147	36%	57%	1%	4%	2% EuF ₃
ZBLAH-144	36%	57%	1%	4%	2% HoF ₃
ZBLAE-331	36%	57%	2.5%	4%	0.5% ErF ₃

thermal experiments were completed, the samples were then polished for the Raman spectroscopy part of the experiment. The samples were polished to a surface layer of one micron with Metadi II diamond polishing compound, made by the Buehler company.

Experimental Setup For Thermal Diffusivity

The experiment was conducted under microcomputer control with the instruments communicating over an IEEE-488 interface bus. The instrumentation consisted of three Hewlett-Packard Model 3478A digital multimeters having a sensitivity of $0.1\mu\text{V}$, a Hewlett-Packard model 3421A data acquisition unit, and a Hewlett-Packard 6284A dc power supply. Three simultaneous readings of the three thermocouples were obtained by sending a group trigger command to the digital voltmeters from the microcomputer approximately every 30 minutes.

The thermocouples were anchored in three shallow grooves spaced at 3 mm intervals and with a small amount of thermally conducting paste (an alumina-filled silicone grease). The shallow (approximately $30\mu\text{m}$) grooves were cut into the samples to hold the three thermometers at equally spaced distances. The thermocouples were then referenced to electronic ice points and connected to the microcomputer. The thermocouples used were 0.003 inch (bare) diameter chromel-alumel thermocouples produced by the Omega Engineering, Inc.. With the same thermal compound, the sample's base was attached to a resistance heater used to obtain a transient temperature distribution in the specimen[2,5].

For measurements above room temperature, the samples were mounted in a small

tube furnace that controlled the mean temperature of the sample. Figure 10 illustrates a schematic representation of the high temperature experimental setup. The tube furnace had an operational range of 300K to 500K with a response time of approximately 5-10 minutes over a large temperature change to obtain the new mean temperature.

For low temperature measurements the sample was mounted on the cold finger of a liquid nitrogen cryostat. Figure 11 illustrates a schematic representation of the low temperature cryostat experimental setup. Notice that the section of cryostat in figure 11 containing the sample is shown enlarged for clarity. The cryostat atmospheric pressure was reduced to nearly zero (~0 atm) to reduce the condensation of moisture on the sample and electronic wires.

Procedure for Thermal Diffusivity

Thermal diffusivity is the preferred technique for studying thermal transport in poor thermal conductors because of its insensitivity to radiate heat losses. The thermal diffusivities were measured using an adaptation of the transient technique developed by Kennedy and coworkers[4]. During each experimental run, simultaneous readings of three thermocouples were obtained by sending a group trigger command to the digital multimeters. With the sample in steady-state conditions temperature readings were taken to establish a “baseline” for the measurement. On command from the computer, the digital relay was closed, supplying current to the transient heater. A constant current was

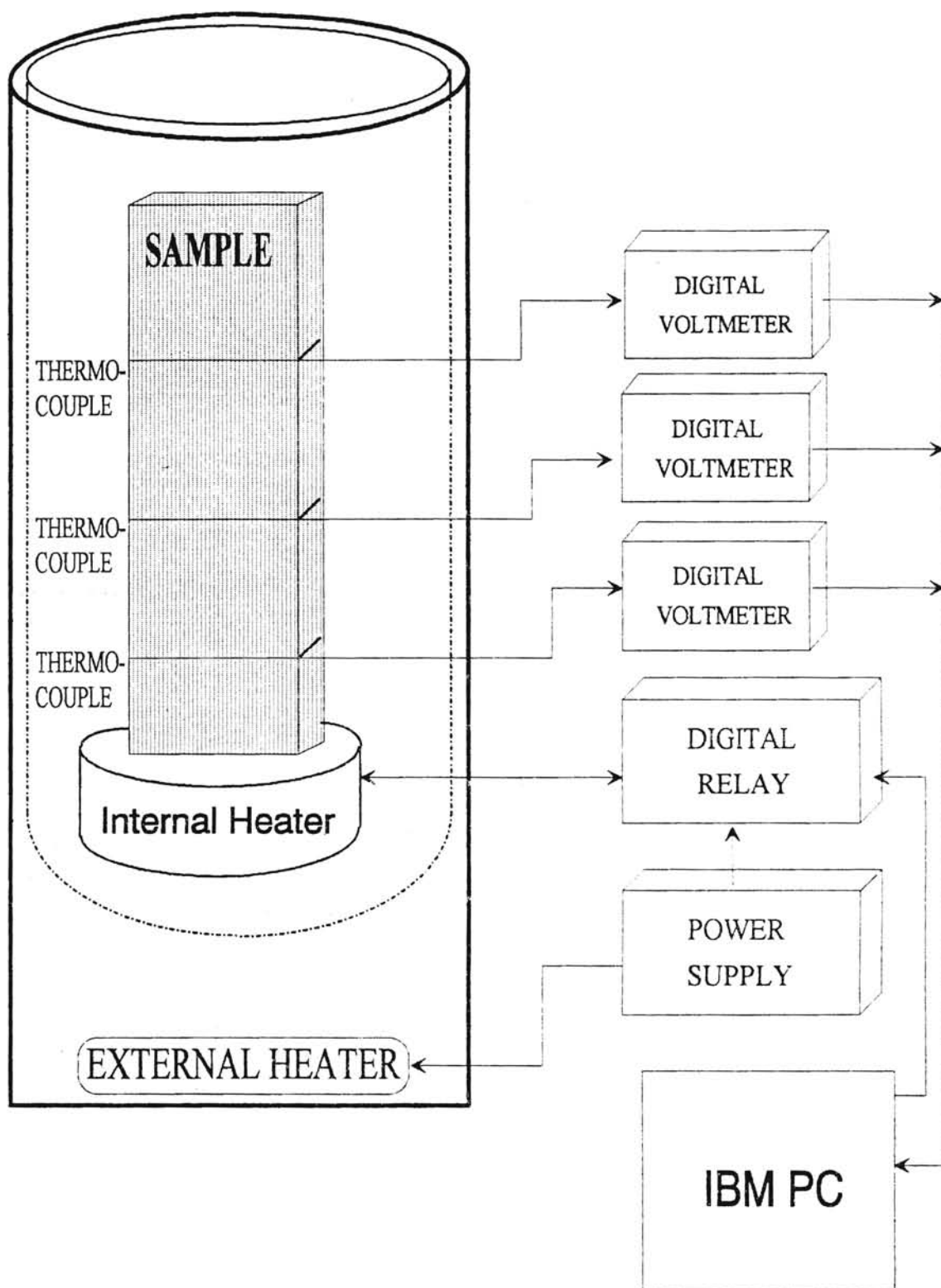


Figure 10. High temperature experimental setup.

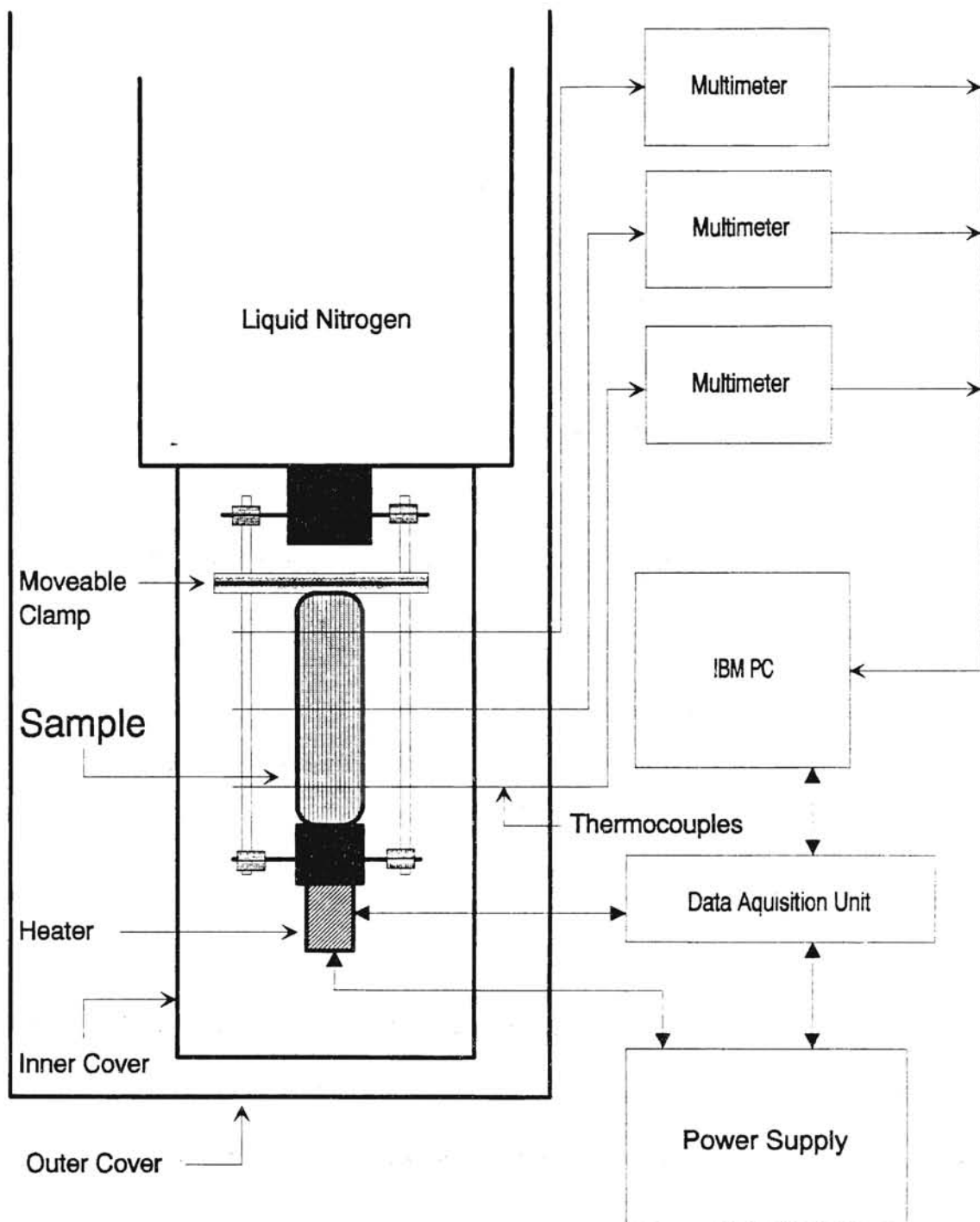


Figure 11. Low temperature experimental setup.

maintained and a 10 second delay was allowed to give the thermocouple the farthest away from the transient heater time to respond. Following the delay, simultaneous temperature measurements were taken by the three thermocouples at intervals of 0.5 seconds. The data was collected for an elapsed time of 50 to 100 seconds. During this time a temperature change of 3 to 8 K occurred at the thermometer closest to the transient heater. At the end of this data-collection interval the relay was opened to turn off the transient heater and allow steady-state conditions to become re-established before the next trial run which occurred 30 minutes later. The purpose for the 30 minute interval between experimental runs was to insure that the transients were given enough time to dissipate. Figure 12 displays a typical data set of temperatures as functions of time for one of the glasses. The upper curve is for the thermocouple closest to the heater and the lower curve is for the thermocouple farthest away from the transient heater.

The thermal diffusivity, α , was obtained from the data using the diffusion equation,

$$\partial T / \partial t = \alpha \nabla^2 T \quad (2-1)$$

This equation was solved for the diffusivity by the computer using a simple algorithm. The algorithm for the diffusivity was evaluated in a few seconds by the microcomputer. Under the assumption of one dimensional heat flow, $\nabla^2 T$ was estimated by the finite difference relation

$$\nabla^2 T_M \approx [(T_U - T_M) - (T_M - T_L)] / (\Delta x^2) \quad (2-2)$$

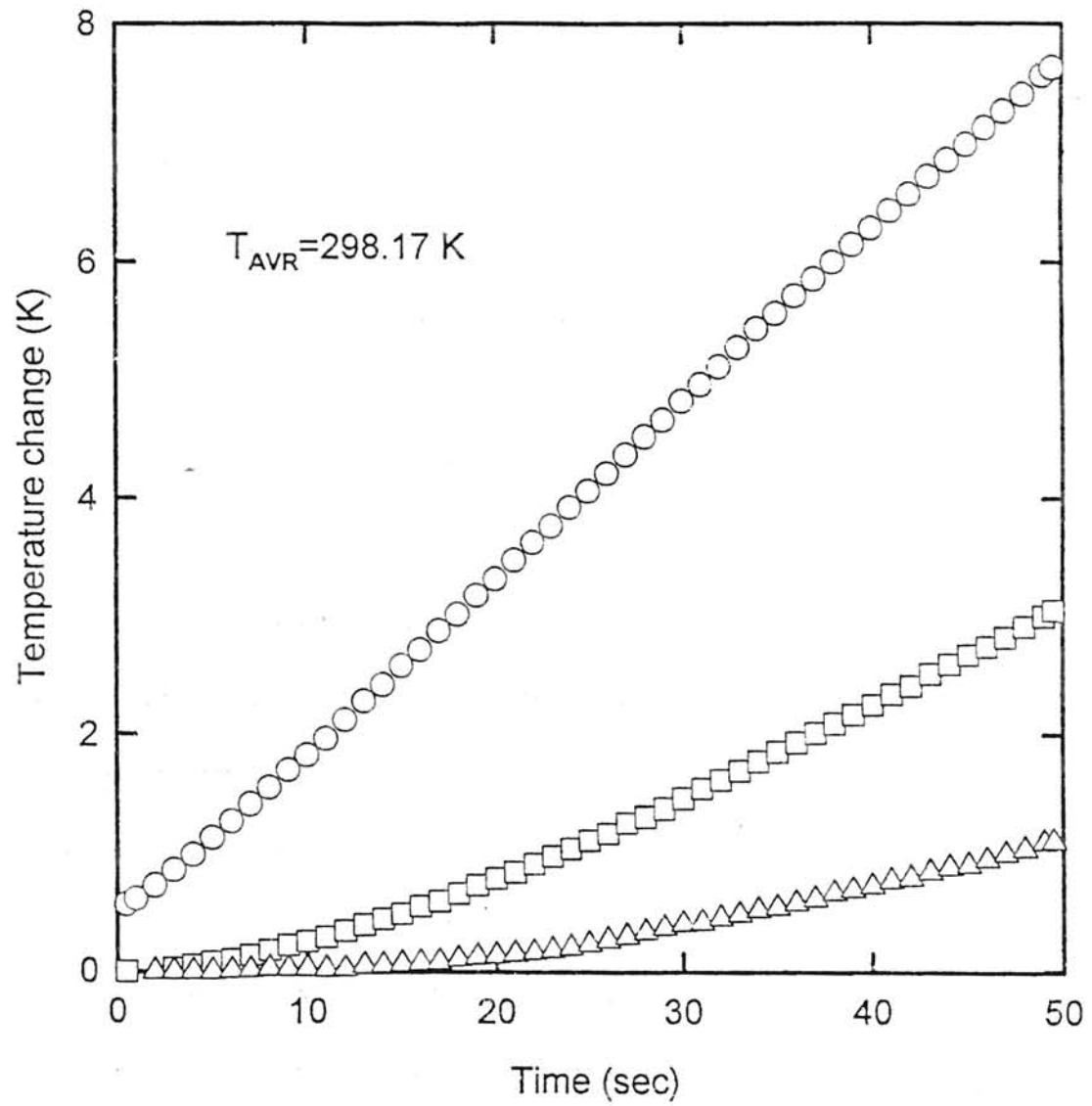


Figure 12. Typical temperature verses time data. The upper curve is for the thermocouple closest to the heater and lower curve is for the thermocouple farthest away from the heater.

for each measurement time in the data set[2]. The subscripts L, M, and U refer to the lower, middle, and upper thermocouples, respectively, while Δx is the spacing between adjacent thermocouples. At each time t_j , $\partial T(t_j) / \partial t$ was estimated by fitting a regression line to a short segment consisting of approximately eight points of $T_M(t)$ on either side of t_j and using the slope of this line as the estimate of the time derivative. The estimates of $\nabla^2 T_M$ were refined by averaging over the same time interval used to evaluate the time derivative[2]. Based on equation (2-1), $\partial T_M / \partial t$ should be a linear function of $\nabla^2 T_M$ with slope α . Figure 13 shows the result of this procedure applied to the data set shown in figure 12. As can be seen in figure 13 the curve is remarkably linear, particularly in view of the number of numerical derivatives that have been performed to generate it[2,5]. The value of α obtained in this way was assigned to the mean temperature of the middle thermocouple during the measurement cycle.

Two kinds of checks have been performed on the reliability of this algorithm to represent the diffusion equation faithfully. First, the method has been used to measure the thermal diffusivities of several standard samples whose known thermal diffusivities cover a broad range of values and which include both amorphous and crystalline solids. In all cases the thermal diffusivities measured by the present technique were in excellent agreement with those reported by Dixon and coworkers[2,5]. A second test was performed on every data set to ensure that the smoothing procedure in the algorithm did not materially affect the estimated thermal diffusivity. The experimental setup was exactly that used by Dixon and coworkers[2]. Based on these checks and the experiment developed by Dixon the method was deemed reliable.

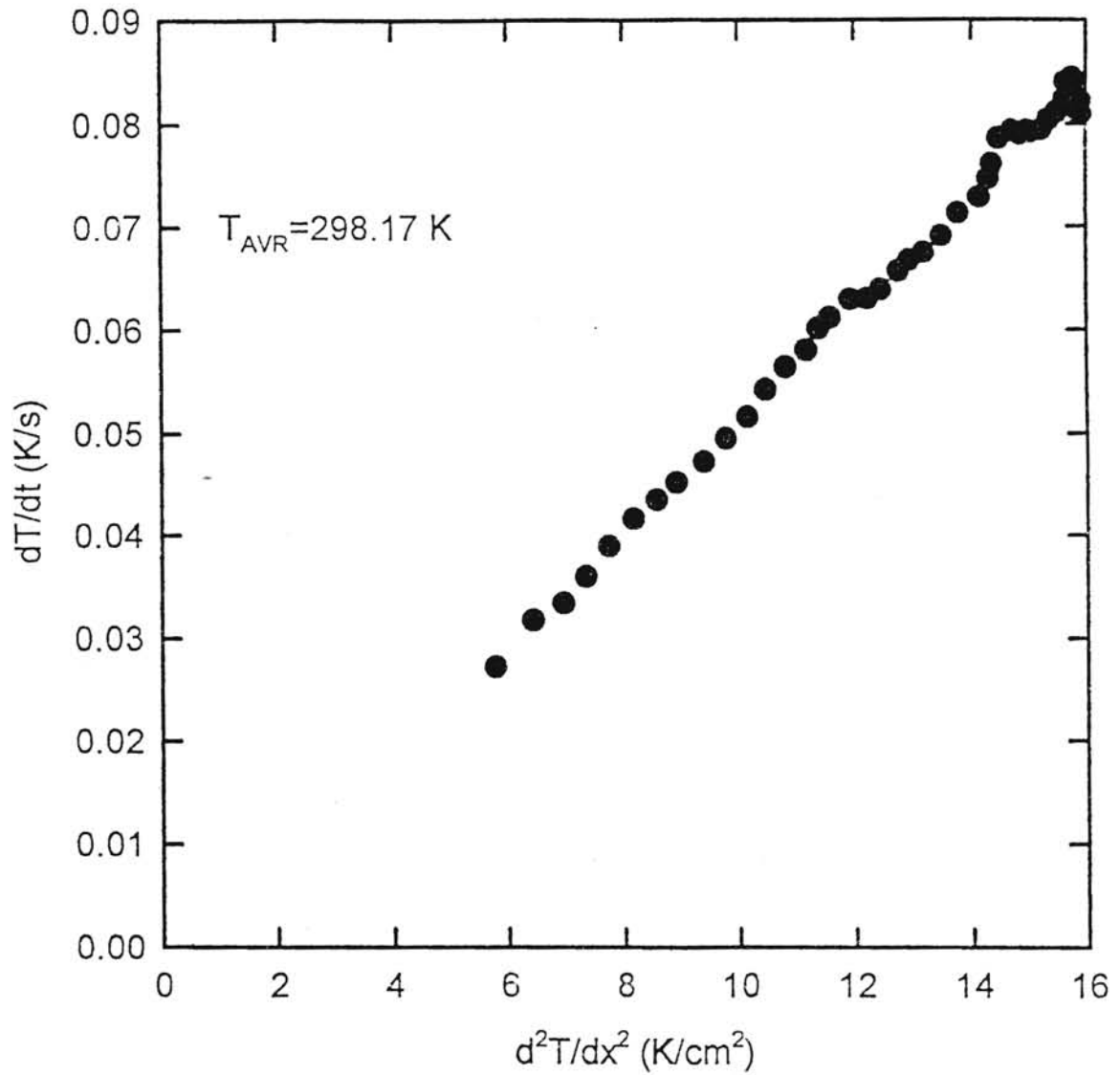


Figure 13. Plot of $\partial T/\partial t$ versus $\partial^2 T/\partial x^2$ calculated from the data of Figure 12. The slope of this curve is the thermal diffusivity, α .

Since temperature was observed at only three locations along the length of the sample, finite difference procedures could not efficiently track $\nabla^2 T$ unless the contributions to the transient temperature distribution from higher order derivatives of the temperature and from radial heat flow were small. This could be guaranteed only if the initial condition of the sample was nearly to steady-state. In the apparatus the best results for these samples were obtained if the transients were allowed to dissipate for 30 minutes between data sets. If this did not agree with the value obtained using the smoothing procedure, the data set was deemed too noisy to be useful.

Experimental Setup For Raman Spectroscopy

The light scattering set up of the Raman spectrometer used in this experiment is shown schematically in figure 14. A Spectra Physics model 2020 Argon-Ion laser was used to produce monochromatic light of wavelength 5145 Å. The power of the laser was variable, from roughly 20 to 500 mW.

The laser output was directed into a Pellin Broca filter system, which allowed the selective transmission of vertically polarized light. Prisms in the system filtered the non-lasing plasma lines by dispersing the light. It was then re-focused by a lens of focal length 300 mm and directed through a pinhole aperture placed 300 mm away. From there, it entered a second lens located 100 mm away, with focal length 100 mm, and was directed

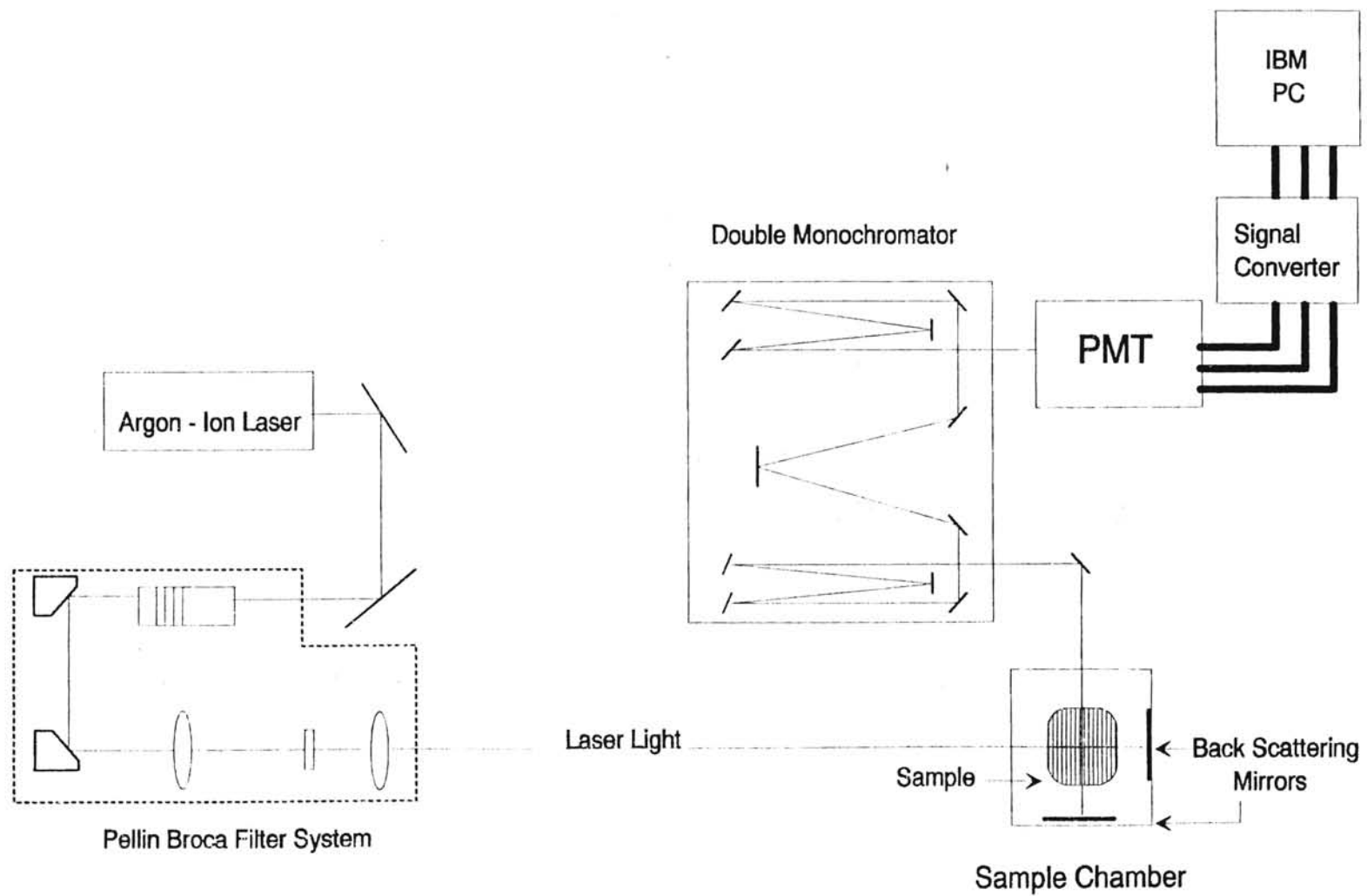


Figure 14. Experimental apparatus for Raman spectroscopy.

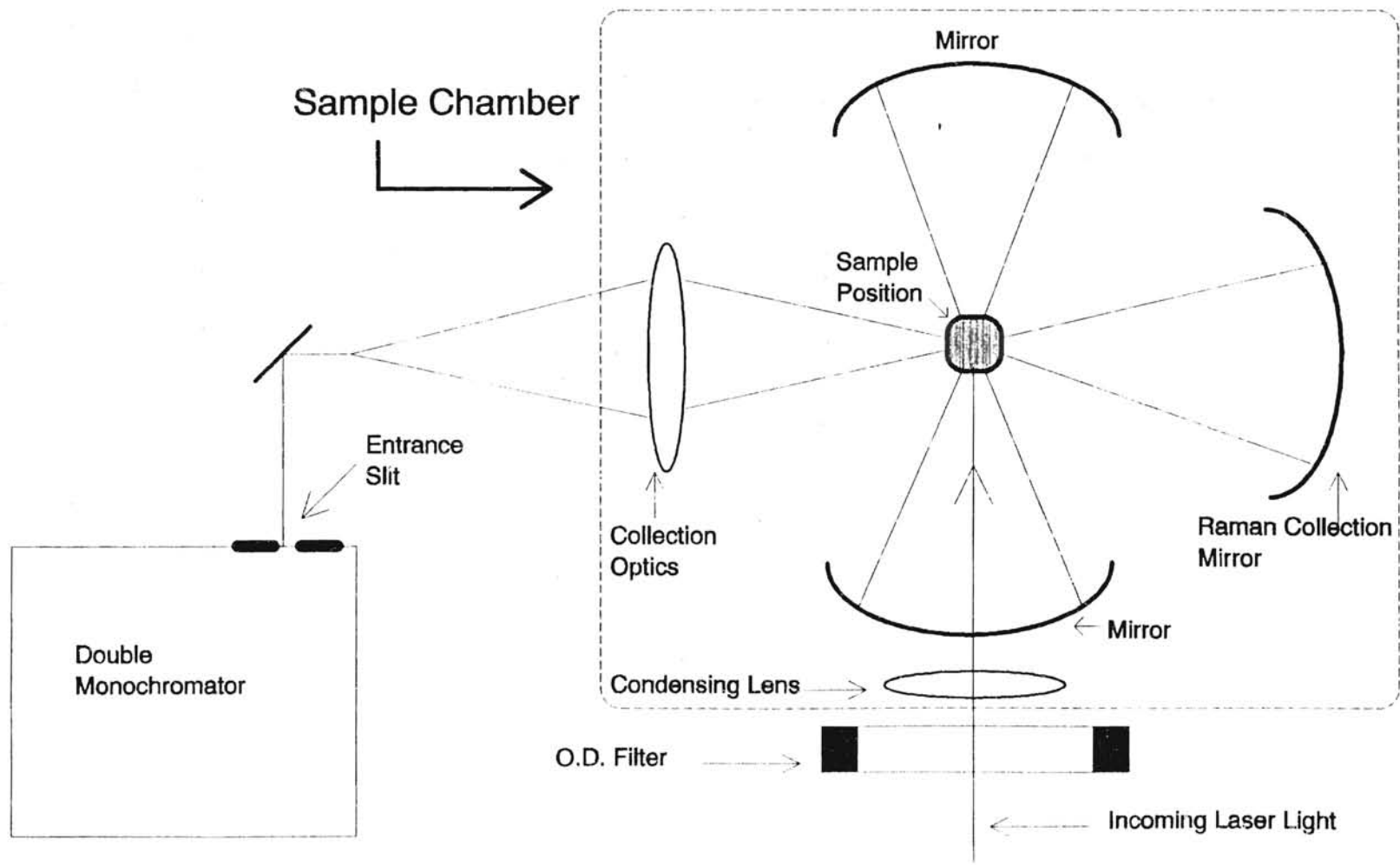


Figure 15. Schematic representation of the sample chamber from Figure 14. (from ref. 9)

method the laser is directed at the sample from the side, top or bottom, and the sample is surrounded by mirrors to reflect as much light as possible into the slit of the spectrometer.

Scattered light was collected in the back scattering configuration, focusing into a Jobin-Yvon Ramanor U-1000 double monochromator. Each monochromator features an asymmetric Czerny-Turner mounting with two symmetrical opening slits. The two diffraction gratings (1800 grooves/mm) rotate on a horizontal shaft parallel to the grating grooves. A concave mirror of focal length 0.5m couples the two monochromators by imaging the exit slit of the first with the entrance slit of the second. Four mirrors, all with focal length 1m, divert the optical paths.

Light exiting the double monochromator was directed into an RCA C31034A photomultiplier tube (PMT) which was cooled to $-20\text{ }^{\circ}\text{C}$ using a Products for Research thermoelectric cooling unit. The PMT was in turn connected to signal converter that was connected to an IBM PC with Enhanced Prism software, used for scanning and analysis. Scans were printed out using a Hewlett-Packard plotter connected to the IBM PC.

Procedure for Raman Spectroscopy

Each day the Raman spectrometer was used, calibration procedures were performed. Within the double monochromator, the mirror coupling the two monochromators and the concave mirror nearest to the exit slit were adjusted to maximize the signal intensity. This was done using a 5461 Å mercury line, created by a mercury lamp, to produce a known Raman peak at the wavenumber of 1122.8 cm^{-1} .

Each sample was first scanned from 5.0 cm^{-1} to 1500 cm^{-1} , with an increment of 1.0 cm^{-1} and integration times between 0.200 to 1.000 seconds. The power of the laser was set at 200 mW whenever possible. However, when this exceeded the computer program capabilities, lower powers of 25mW to 100mW had to be used. Peaks of interest were scanned over a narrower range of wavenumbers with a smaller increment and longer integration time, resulting in increased accuracy. Enhanced Prism software was used to determine the positions of peaks and their full widths at half the maximum of the peak heights. All scans were saved on the IBM PC hard drive and could be plotted out or examined at a later time.

CHAPTER III

RESULTS and DISCUSSION

The thermal diffusivities of the three samples are shown as a function of temperature in figures 16 through 18. Figure 19 displays the diffusivity of the samples on a single graph. As can be expected the curves are all very similar in form with the uppermost curve representing the sample with Holmium doping, the middle curve representing the Europium doping and the lowermost curve representing the sample with Erbium doping.

The model used to describe the data has been proposed by Dixon and coworkers[2,5] where thermal transport is represented by a two-carrier model of conventional phonon-gas transport by extended phonons and thermally activated hopping of localized phonons. In this model, the extended phonons produce a transport that is a decreasing function of temperature between 100 and 250K, while the localized phonons produce a transport that is a linearly increasing function of temperature above 250K[5]. While this model employs many of the ideas inherent in the fracton model proposed by Orbach and coworkers[12,13,14], it differs in that a fractal nature of glasses is not assumed. Instead, empirical properties of the glasses are used to support the analysis.

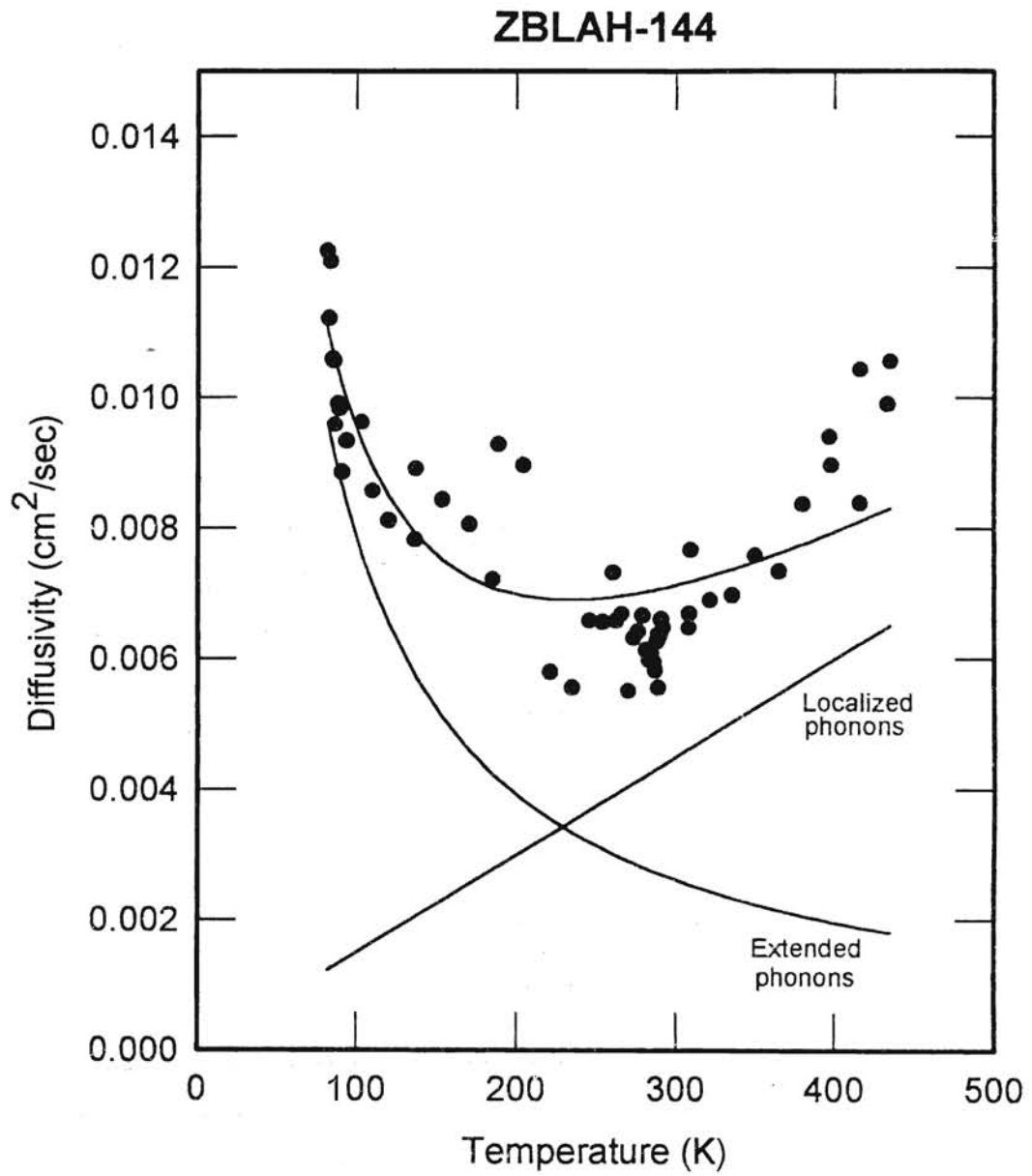


Figure 17. Thermal diffusivity as a function of temperature for the ZBLAH-144 sample. In addition, the individual contributions to the thermal diffusivity of the extended and localized phonons is shown.

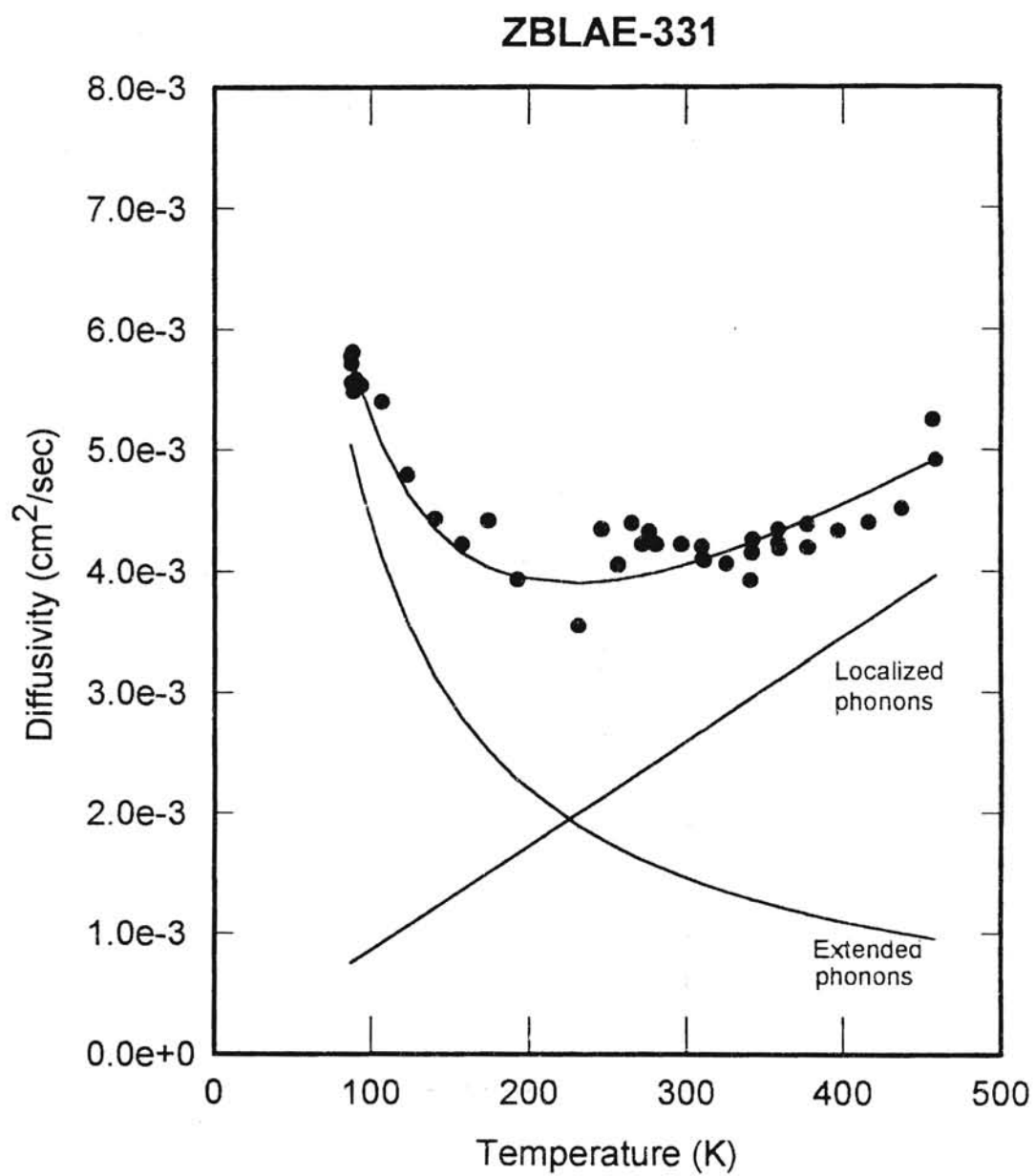


Figure 18. Thermal diffusivity as a function of temperature for the ZBLAE-331 sample. In addition, the individual contributions to the thermal diffusivity of the extended and localized phonons is shown.

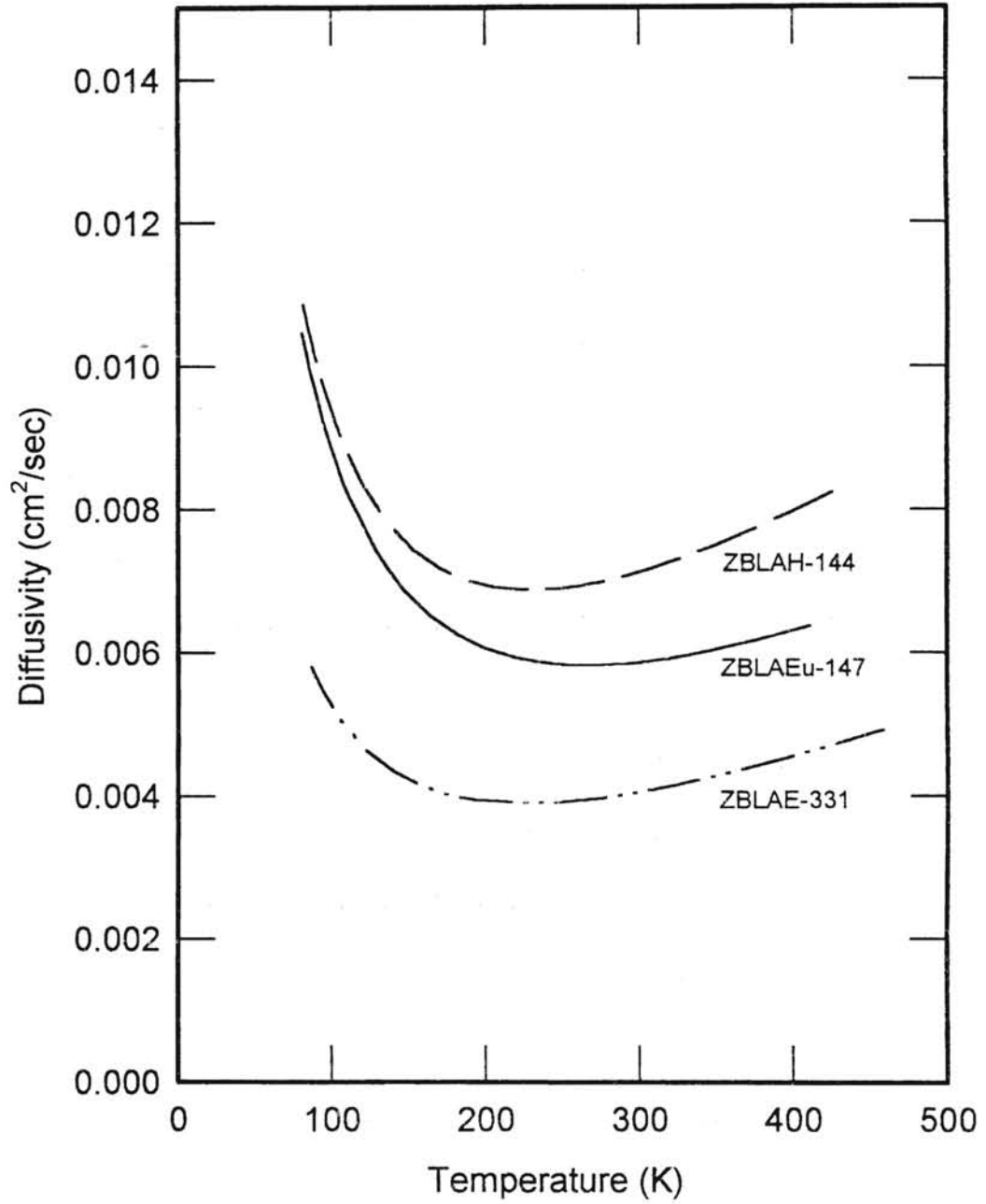


Figure 19. The thermal diffusivities as a function of temperature for all three samples.

Table 2 lists the relevant physical properties of the glasses used in this analysis. In particular, the concept of a “formula unit” was employed. The “formula unit” was first introduced by Dixon and coworkers[2] and is defined as the smallest number of atoms in which each element is represented in the same proportion as in the sample as a whole. Since the glasses studied here are mixtures rather than compounds, the “formula units” are not whole numbers. We shall retain the quotation marks as a reminder of this fact. The molar volume is the ratio of mass of the “formula unit” to the density of the sample. Table 2 also includes the sound velocity, 3.00×10^5 cm/s, which was used for all three samples. This value was taken from a sample in reference 5 which was very similar in composition to the sample glasses in this experiment.

From the Raman spectroscopy scattering experiments the existence of low frequency extended phonons and localized phonons was inferred. The Raman spectra for the samples are shown in figures 20 to 22. The onset of Raman activity is interpreted to represent phonon localization with the cutoff frequency, ω_c , separating the extended phonons from the localized ones[2]. While Dixon and coworkers[2,5] define the boson peak in the Raman data as representing the mobility edge (cutoff frequency), this experiment utilizes the minimum preceding the boson peak as representing the mobility edge.

Based on the two-carrier model, the thermal diffusivity due the extended phonons and the localized phonons can be written as

$$\alpha = \frac{1}{3} \frac{C_{ext}}{C} v^2 \tau_{ext} + \frac{C_{loc}}{C} \frac{\langle R^2 \rangle}{\tau_{loc}} \quad (3-1)$$

TABLE II. Physical properties of the glasses.

Modifier	ZBLAEu-147	ZBLAH-144	ZBLAE-331
Density (g/cm ³)	4.08	4.03	3.95
Formula Mass (u) or Molecular Weight (g/mol)	16,792.8	16,818.7	33,219.7
N ₀ (Smallest # of atoms in formula unit)	421	421	842
Molar Volume (cm ³ /mole)	4112.2	4175.8	8415.7
Average sound velocity of extended phonons, v _s (10 ⁵ cm/s)	3.0	3.0	3.0
Cutoff frequency, ω _c , in wavenumbers (cm ⁻¹)	16	16	15
Cutoff frequency, ω _c (10 ¹² Hz)	0.485	0.485	0.455
Raman Frequencies (cm ⁻¹)			
ω ₁ (cm ⁻¹) / ω _c (10 ¹² Hz)	45.0 / 1.36	45.0 / 1.36	150.0 / 4.54
ω ₂ (cm ⁻¹) / ω _c (10 ¹² Hz)	186.0 / 5.60	185.0 / 5.60	276.0 / 8.36
ω ₃ (cm ⁻¹) / ω _c (10 ¹² Hz)	583.0 / 17.6*	275.0 / 8.33	508.0 / 15.39
ω ₄ (cm ⁻¹) / ω _c (10 ¹² Hz)	666.0 / 20.18	585.0 / 17.73	944.0 / 28.61
ω ₅ (cm ⁻¹) / ω _c (10 ¹² Hz)	751.0 / 22.75	1025 / 31.1*	997.0 / 30.21
ω ₆ (cm ⁻¹) / ω _c (10 ¹² Hz)	804.0 / 24.36	1205 / 36.51	1252 / 37.94
ω ₇ (cm ⁻¹) / ω _c (10 ¹² Hz)	1378 / 41.7*	N/A	N/A
Heat Capacity, C (J/K-cm ³)	12.11	11.93	13.77
Heat Capacity for extended phonons, C _{ext} (10 ⁻⁶ J/K-cm ³)	2.95	2.95	2.44
C _{ext} /C (10 ⁻⁷)	2.43	2.47	1.77
A (10 ⁶ cm ² K/s)	3.19	3.18	2.48
B (10 ⁻⁵ cm ² /s-K)	1.09	1.50	0.864

Note: *Data excluded due to electronic transition states.

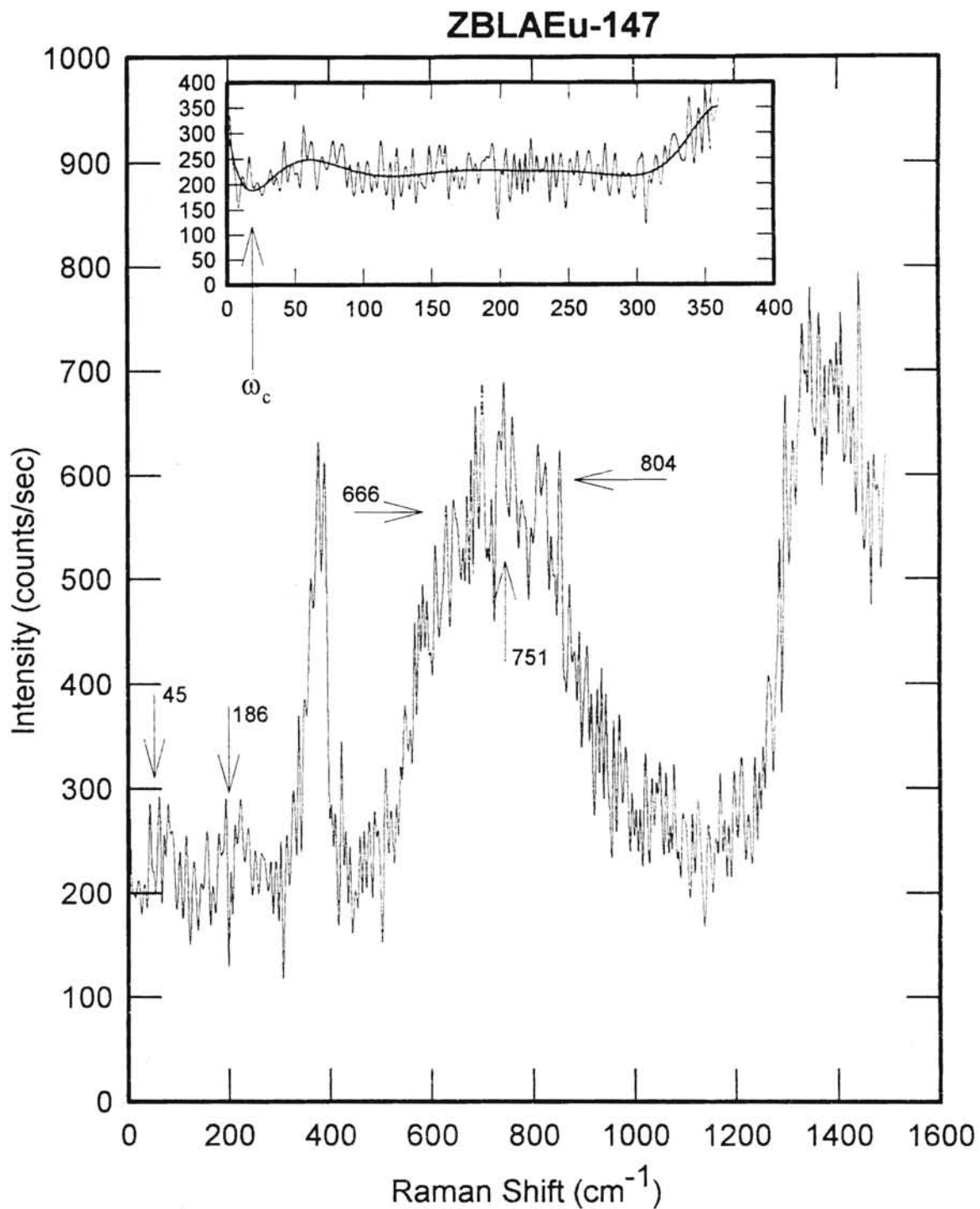


Figure 20. Raman spectrum of the ZBLAEu-147 sample. The main figure shows the full Raman spectrum for this sample. The arrows in the full spectrum point to the frequencies used in the multi-term Einstein approximation.

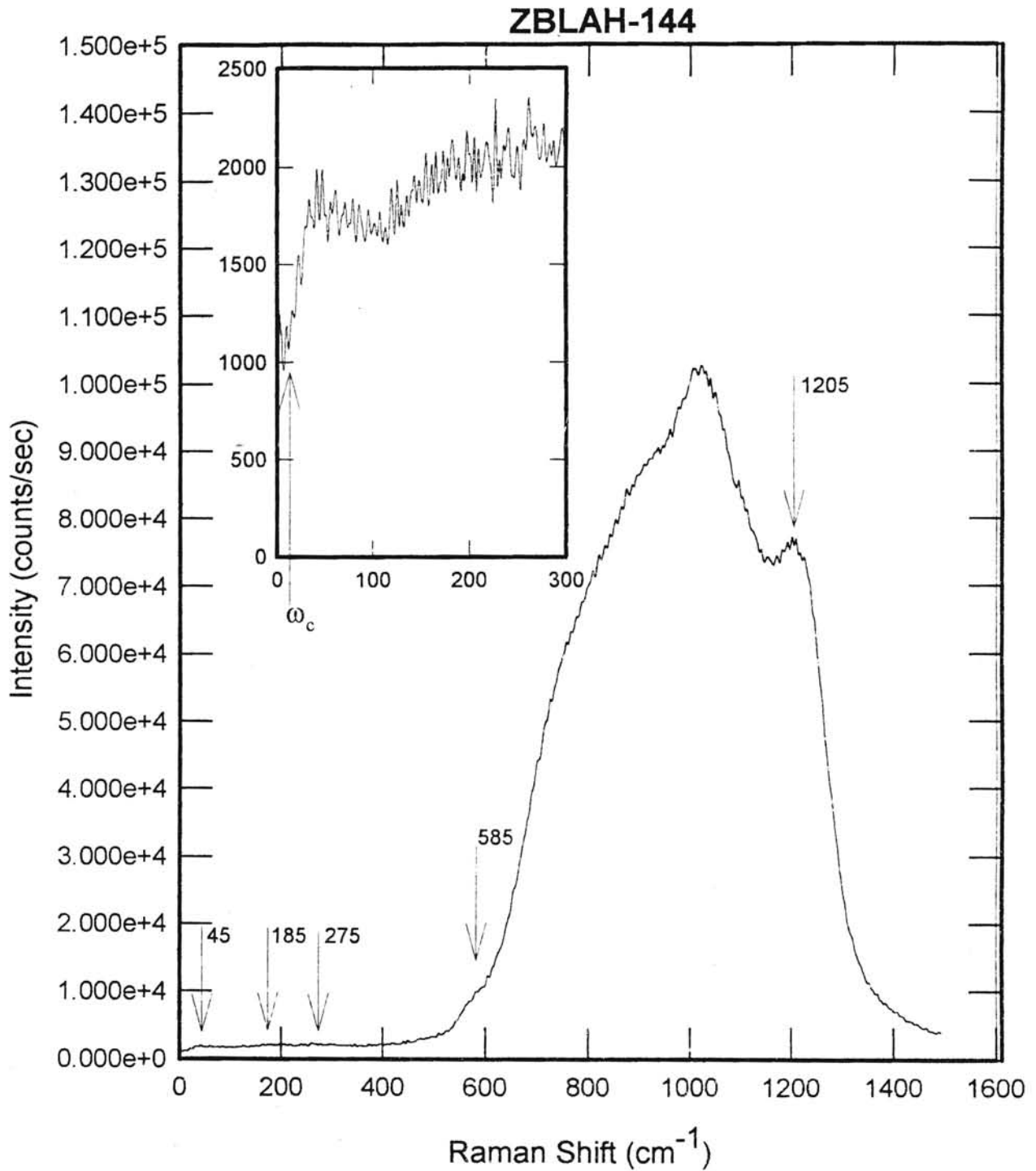


Figure 21. Raman spectrum of the ZBLAH-144 sample. The main figure shows the full Raman spectrum for this sample. The arrows in the full spectrum point to the frequencies used in the multi-term Einstein approximation.

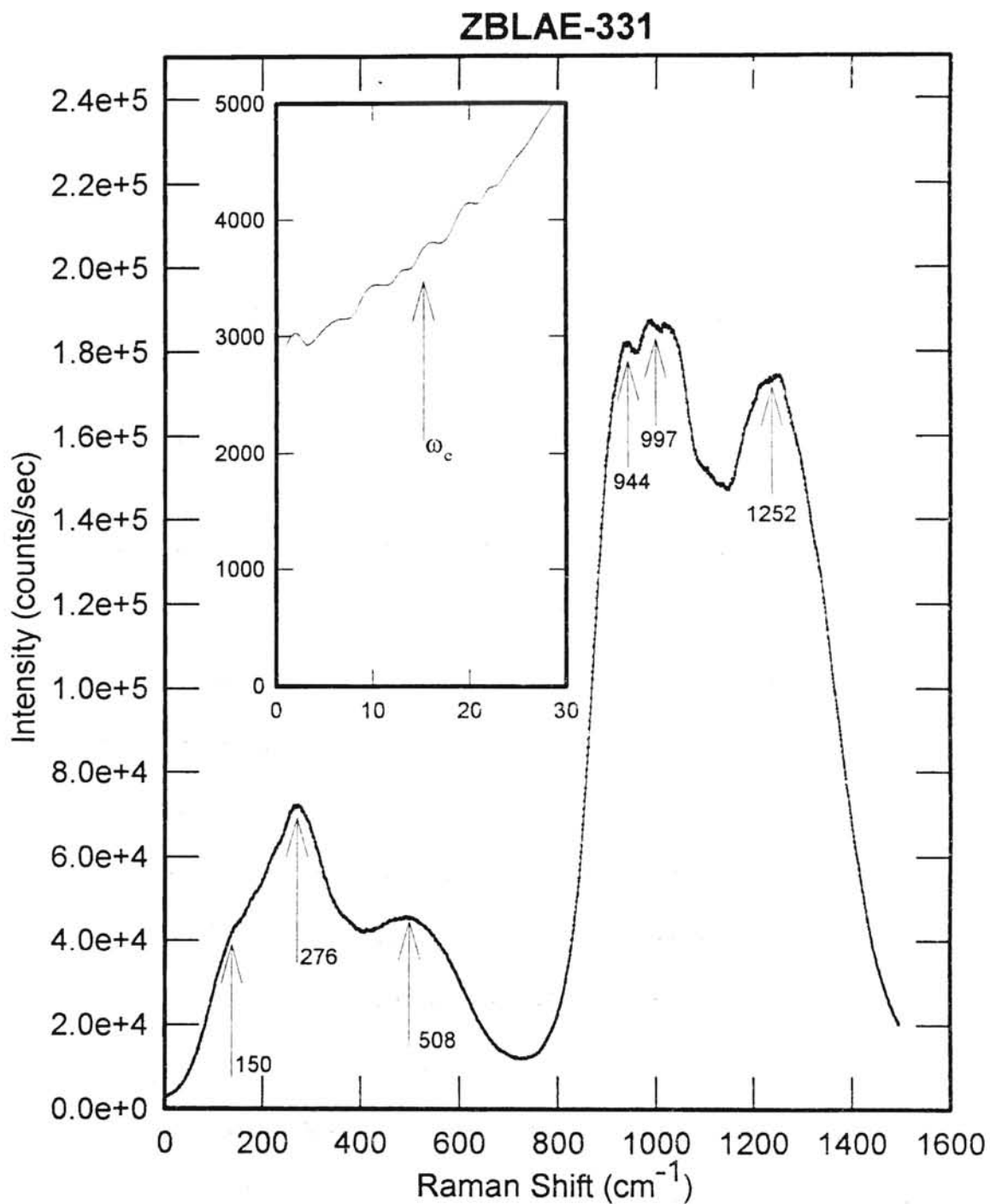


Figure 22. Raman spectrum of the ZBLAE-331 sample. The main figure shows the full Raman spectrum for this sample. The arrows in the full spectrum point to the frequencies used in the multi-term Einstein approximation.

where the first term represents the contribution due to extended phonons and the second term the contribution due to the thermally activated hopping of localized phonons. C_{ext} and C_{loc} are the heat capacity per unit volume of the extended and localized phonons, respectively, and $C=C_{ext}+C_{loc}$. The terms τ_{ext} and τ_{loc} are the mean lifetimes of the extended and localized phonons, respectively, and v_s is the velocity of sound in the samples. $\langle R^2 \rangle$ represents the thermally averaged square hopping distance. Replacing C_{loc} with $C-C_{ext}$, equation (3-1) becomes

$$\alpha = \frac{1}{3} \frac{C_{ext}}{C} v_s^2 \tau_{ext} + \left(1 - \frac{C_{ext}}{C}\right) \frac{\langle R^2 \rangle}{\tau_{loc}} \quad (3-2)$$

If phonon-phonon scattering is assumed to be the dominant resistive anharmonic process for the extended phonons then $\tau_{ext} \propto T^{-1}$ can be used to fit the data[2,5]. On the other hand, the phenomenon referred to as “hopping” by Dixon and coworkers[2,5] is the major contributor of the localized modes to the thermal transport. “Hopping” is defined as a three phonon anharmonic process where an extended phonon is scattered by a localized phonon to produce another localized phonon. The reverse of this process, in which an extended phonon is produced when a localized phonon scatters another localized phonon, may also occur. In this process energy conservation dictates that if a localized phonon decays, it must reappear a distance R away in some other mode in the glass. Since the disorders of the glasses leads to a distribution of localized phonon frequencies where neighboring modes will most likely vary in frequency, a low frequency extended phonon will be emitted or absorbed to make up the energy difference between the donor localized modes and the acceptor localized modes[2]. This three phonon anharmonic process is illustrated schematically in figure 23. Orbach and coworkers[12,13,14] have

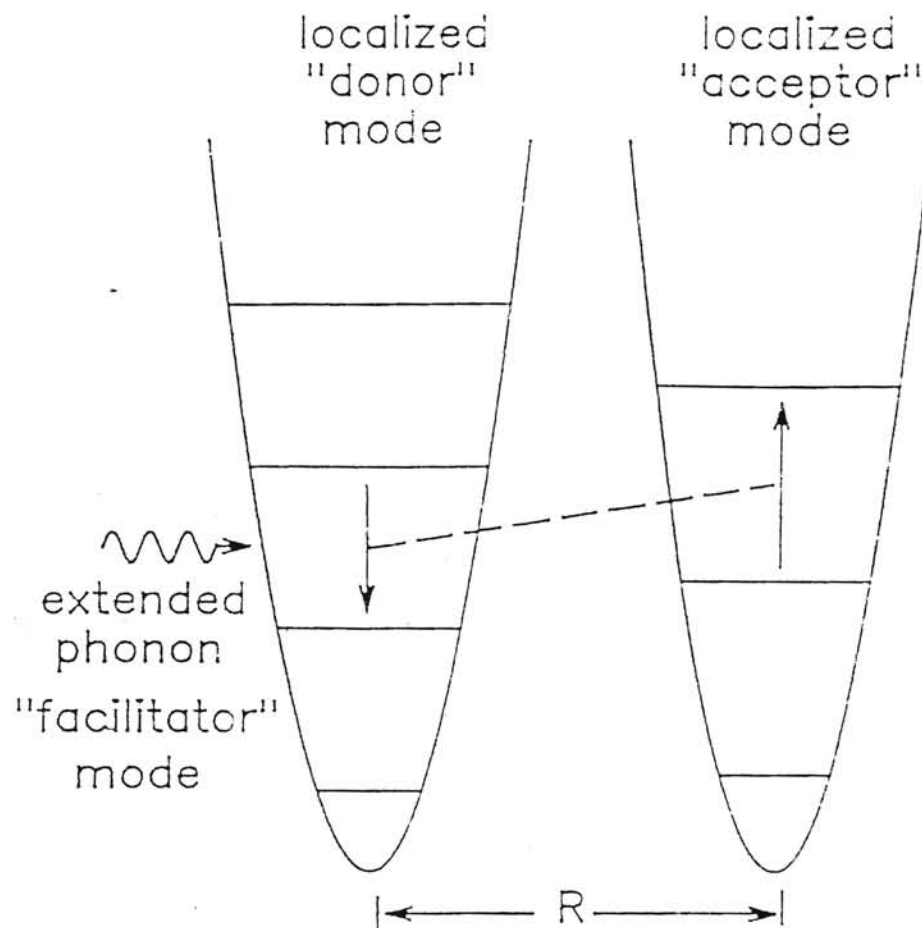


Figure 23. Schematic representation of the thermally activated hopping of localized phonon process.

demonstrated through their fractal model that this three phonon process contributes a localized thermal diffusivity that is a linear function of temperature to the total thermal diffusivity, $\alpha = \alpha_{\text{ext}} + \alpha_{\text{loc}}$. Keeping this in mind and the assumption that $\tau_{\text{ext}} \propto T^{-1}$, the functional equation used to fit the data is

$$\alpha = \frac{C_{\text{ext}}}{C} AT^{-1} + \left(1 - \frac{C_{\text{ext}}}{C}\right) BT \quad (3-3)$$

where A and B are constants to be determined by the fit.

In determining the heat capacity of the extended phonons, a Debye approximation was used at the high temperature limit for these modes. This approximation gives the extended phonon heat capacity as

$$C_{\text{ext}} = \left(\frac{w_c}{v_s}\right)^3 \frac{k_B}{(2\pi^2)} \quad (3-4)$$

Since the peaks in the Raman spectra extend to roughly 1600cm^{-1} , a multi-term Einstein approximation was used for the determination of the total heat capacity, C, to correct for the temperature variation of this total heat capacity. This was accomplished by approximating the phonon density of states by the center frequencies of the six Raman peaks and substituting these frequencies in the equation

$$C = 3nk_B \left(\frac{\hbar}{k_B T}\right)^2 \sum_{i=1}^n \left(\frac{\omega_i^2 e^{\hbar\omega_i/k_B T}}{(e^{\hbar\omega_i/k_B T} - 1)^2}\right) \quad (3-5)$$

where n, the number of modes per unit volume was taken as the ratio of the “formula unit” to the molar volume and T was set equal to each corresponding Raman peak temperature. The values for C, C_{ext} , and the ratio C_{ext}/C together with the constants A and B are listed in table 2. Note that some of the raman peaks were deliberately excluded due to

electronic transition states of the rare earth elements used during this experiment. It is worth mentioning that, had the mobility edge been approximated by the boson peak in the Raman spectra as was done in references 2 and 5, the values for the ratio C_{ext}/C calculated would have been similar to the values calculated for the families of glasses studied by Dixon and coworkers[2,5].

In examining the thermal diffusivities in figure 19, they are observed to increase linearly at room temperature and above, while below room temperature the thermal diffusivities are a decreasing function of the temperature. This behavior is similar to the behavior described in reference 5 for the same family of glasses. This is to be expected since the samples studied in this experiment are very similar to one of the samples studied in reference 5. In contrast, the behavior of the thermal diffusivities of the family of glasses studied in reference 2 shows that the thermal diffusivities are roughly linear in temperature throughout the whole temperature region studied here, in reference 2, and in reference 5. Dixon and coworkers[2,5] suggested that the extended phonons in the samples in this study and in reference 5 make a larger contribution, relative to the localized phonons, to the thermal diffusivity due to weaker anharmonic interactions in these samples compared to stronger anharmonic interactions in the samples studied in reference 2. The weaker anharmonic interactions in the glasses studied here and in reference 5 are assumed to affect the behavior of the thermal diffusivity in two ways. First, since anharmonic interactions are weaker, less phonon-phonon scattering takes place, allowing the extended phonons to make a larger contribution to the thermal diffusivity. Second, the weaker anharmonic interactions mean that the contribution to the thermal diffusivity by the localized phonons is reduced since they are more weakly coupled to extended phonons

which serve to facilitate thermally activated hopping of these modes[5]. The reasons why the anharmonic interactions in the glasses studied here and in reference 4 are weaker than in the glasses studied in reference 2 is unclear. Further studies may reveal that this is possibly accounted for by the structures of the glasses.

The two-carrier model can also help to explain why the different doping concentrations of europium, erbium, and holmium have a stronger effect on the thermal diffusivities at temperatures above room temperatures than at temperatures below. If the two-carrier model is correct in asserting that the density of states of the samples is such that it contains extended phonons, and above a mobility edge, ω_c , localized phonons, then at low temperatures, where the phonons are mostly extended modes, we do not expect the increases in the density fluctuations introduced by the different doping concentrations to affect these modes since the extended phonon wavelengths are large enough that they are essentially insensitive to the increase in density fluctuations. On the other hand, at higher temperatures where extended phonon wavelengths approach a length scale comparable to the length scale of the disorder in the glasses, the increases in the density fluctuations become more apparent thereby introducing scattering centers which ultimately cause the thermal diffusivity to decrease. This is supported by the fact that the masses of the three different samples are much more massive, respectively, than any of the other elements present in the samples in this study.

CHAPTER IV

CONCLUSION

In this experiment the thermal diffusivities of a set of three glasses were studied as a function of temperature. The glasses studied were ZBLAEu-147, ZBLAH-144, and ZBLAE-331. The two samples named ZBLAEu-147 and ZBLAH-144 consisted of a base compositional formula of $0.36(\text{BaF}_2) 0.57(\text{ZrF}_4) 0.01(\text{LaF}_3) 0.04(\text{AlF}_3) 0.02(\text{M})$ and doped with the modifier (M) of EuF_3 or HoF_3 , respectively. The third sample, ZBLAE-331, had the same composition as the other two with the exception of $0.025(\text{LaF}_3)$ and the modifier(M) being 0.05ErF_3 .

It was shown that, based on the two-carrier model proposed by Dixon and coworkers[2,5], the thermal diffusivity data can be explained fairly well. In this model, the dominant thermal transport mechanism below a mobility edge is through extended state phonons, while above this mobility edge localized phonons interacting with extended phonons through a three phonon anharmonic process acts as the main contributor to the thermal diffusivity. The fact that above room temperature, the thermal diffusivity is seen to be linearly dependent on temperature seems to support this hypothesis.

On the other hand, for temperatures below room temperatures, if phonon-phonon scattering is assumed to be the main process to the thermal transport by the means of extended phonons, then the thermal diffusivity can be described as a decreasing function of temperature, which describes the data well. Furthermore, the thermal diffusivities'

decreasing nature supports the existence of a phonon spectrum that contains both extended phonons and, above the mobility edge, ω_c , localized phonons.

In this analysis the mobility edge and the frequencies of the localized phonon modes were obtained from Raman data which, together with a Debye and Einstein approximation, were used to calculate the total heat capacity and the heat capacity of the extended phonons

REFERENCES

- [1] R. C. Zeller and R. O. Pohl, *Phys. Rev. B* **4**, 2029 (1971).
- [2] G. S. Dixon, B. D. Gault, J. P. Wicksted, P. A. Watson, and Shu-yun Shi, *Phys. Rev. B* **49**, 257 (1994).
- [3] *Amorphous Solids*, edited by W. A. Phillips (Springer-Verlag, Berlin, 1981)
- [4] W. L. Kennedy, P. H. Sidles, and G. C. Danielson, *Direct Energy Conversion* **2**, 53 (1962).
- [5] W. P. Allen, L. Devlin, T. Doyle, R. Sinder, P. A. Watson, and G. S. Dixon, *Phys. Rev. B* **49**, 264 (1994).
- [6] *The Physics of Amorphous Solids* by Zallen, Richard (John Wiley & Sons, Inc., US 1983).
- [7] *Defects and Disorder in Crystalline and Amorphous Solids*, edited by C. R. A. Catlow (Kluwer Academic Publishers, Netherlands 1994).
- [8] Gilson, T. R., and Hendra, P. J. *Laser Raman Spectroscopy*. Bath, Great Britain: Dawson and Goodall Ltd., The Mendip Press, 1970.
- [9] Loader, J. *Basic Laser Raman Spectroscopy*. New York, New York, Heyden & Son Ltd., 1970.
- [10] B. Golding, J. E. Graebner, and L. C. Allen, *Phys. Rev. B* **34**, 5696 (1986).
- [11] D. Walton, *Solid State Commun.* **14**, 335 (1974).
- [12] S. Alexander, O. Entin-Wohlman, and R. Orbach, *Phys. Rev. B* **34**, 2726 (1986)
- [13] R. Orbach, *J. Non-Cryst. Sol.* **164**, 917 (1933).
- [14] A. Jagannathan, R. O. Orbach, and O. Entin-Wohlman, *Phys. Rev. B* **39**, 13465 (1989).
- [15] *Interaction of Phonons with Photons: Infrared, Raman, and Brillouin Spectra*, edited by T. A. Bak (W. A. Benjamin, Inc., New York 1964).

- [16] S. Alexander, C. Laermans, R. Orbach, and H. M. Rosenberg, *Phys. Rev. B* **28**, 4865 (1983).
- [17] D. G. Cahill and R. O. Pohl, *Ann. Rev. Phys. Chem. B* **39**, 93 (1988).
- [18] A. T. Petit and P. L. Dulong, *Ann. Chim. Phys. (2nd Ser.)* 10: 395, 1819.
- [19] H. F. Weber, *Ann. Phys.* **154**: 367, 553, 1875.
- [20] A. Einstein, *Ann. Phys.* **22**: 180, 1907.
- [21] P. Debye, *Ann. Phys.* **39**: 789, 1912.
- [22] M. Born and von Karman, *Phys. Rev. Z* **13**: 297, 1912.
- [23] *Vortraege ueber die Kinetische Theorie der Materie und der Elektrizitaet*, P. Debye, Berlin: Teubner, 1914.
- [24] R. E. Peierls, *Ann Phys.* **3** 1055, 1929.
- [25] P. W. Anderson, B. I. Halperin, C.M. Varma, *Philos. Mag.* **25**: 1.
- [26] W. A. Phillips, *Low Temp. Phys.*, **7**: 351.
- [27] *Effects of Modes of Formation on the Structure of Glasses*, edited by R. A. Weeks and D.L. Kinser, pp. 305-414 (Trans Tech Publications Ltd, Switzerland 1987).

VITA 2

John F. Snodgrass

Candidate for the Degree of

Master of Science

Thesis: THERMAL DIFFUSIVITY IN FLUORIDE GLASSES

Major field: Physics

Biographical:

Personal Data: Born in Berea, Ohio, on January 25, 1969.

Education: Graduated from Berea High School, Berea, Ohio, in June 1987. Received the Bachelor of Science degree in Physics from Edinboro University of Pennsylvania at Edinboro in May 1991. Completed the requirements for the Master of Science in Physics from Oklahoma State University in May, 1996.

Professional Experience: Graduate Research Assistant, Oklahoma State University, May 1994 to present. Graduate Teaching Assistant, Oklahoma State University, August 1993 to May 1995. Research Assistant and Laboratory Technician, Edinboro University of Pennsylvania, August 1989 to May 1991.